Screening Mycobacterium tuberculosis secreted proteins identifies Mpt64 as eukaryotic membrane-binding virulence factor

Chelsea E. Stamm[a,b], Breanna L. Pasko[a,b], Sujittra Chaisavaneeyakorn[a,c], Luis H. Franco[a,d]*, Vidhya R. Nair[a], Bethany A. Weigele[b]*, Neal M. Alto[b], Michael U. Shiloh[a,b]#.

[a]Department of Internal Medicine, University of Texas Southwestern Medical Center, Dallas, Texas, USA

[b]Department of Microbiology, University of Texas Southwestern Medical Center, Dallas, Texas, USA.

[c]Department of Pediatrics, University of Texas Southwestern Medical Center, Dallas, Texas, USA.

[d]Center for Autophagy Research, University of Texas Southwestern Medical Center, Dallas, Texas USA

Running title: Mtb Mp64 is a membrane-binding virulence factor

#Address correspondence to Michael U. Shiloh, michael.shiloh@utsouthwestern.edu

*Present address: Luis Franco, Federal University of Minas Gerais, Belo Horizonte, Brazil; Bethany Weigele, Arizona State University, Scottsdale, Arizona USA.

Abstract word count: 203

Text word count: 7,901

Abstract

Mycobacterium tuberculosis (Mtb), the causative agent of tuberculosis, is one of the most successful human pathogens. One reason for its success is that Mtb can reside within host macrophages, a cell type that normally functions to phagocytose and destroy infectious bacteria. However, Mtb is able to evade macrophage defenses in order to survive for prolonged periods of time. Many intracellular pathogens secret virulence factors targeting host membranes and organelles to remodel their intracellular environmental niche. We hypothesized that Mtb exported proteins that target host membranes are vital for Mtb to adapt to and manipulate the host environment for survival. Thus, we characterized 200 exported proteins from Mtb for their ability to associate with eukaryotic membranes using a unique temperature sensitive yeast screen and to manipulate host trafficking pathways using a modified inducible secretion screen. We identified five Mtb exported proteins that both associated with eukaryotic membranes and altered the host secretory pathway**.** One of these secreted proteins, Mpt64, localized to the endoplasmic reticulum during Mtb infection of murine and human macrophages and was necessary for Mtb survival in primary human macrophages. These data highlight the importance of exported proteins in Mtb pathogenesis and provide a basis for further investigation into their molecular mechanisms.

Importance

Advances have been made to identify exported proteins of *Mycobacterium tuberculosis* during animal infections. These data, combined with transposon screens identifying genes important for *M. tuberculosis* virulence, have generated a vast resource of

potential *M. tuberculosis* virulence proteins. However, the function of many of these proteins in *M. tuberculosis* pathogenesis remains elusive. We have integrated three cell biological screens to characterize nearly 200 *M. tuberculosis* exported proteins for eukaryotic membrane binding, host subcellular localization and interactions with host vesicular trafficking. In addition, we observed the localization of one exported protein, Mpt64, during *M. tuberculosis* infection of macrophages. Interestingly, although Mpt64 is exported by the Sec pathway, its delivery into host cells was dependent upon the action of the Type VII Secretion System. Finally, we observed that Mpt64 contributes to the virulence of *M. tuberculosis* during infection of primary human macrophages.

Introduction

Tuberculosis caused by *Mycobacterium tuberculosis* (Mtb) is a persistent, global epidemic. While the number of deaths due to Mtb fell below 2 million in 2015, there were over 9 million new cases (1) and the incidence of multidrug-resistant Mtb is increasing (1), highlighting the need for new anti-tuberculosis therapies. In addition, the only currently available vaccine, *Mycobacterium bovis* Bacille-Calmette-Guérin (BCG), is ineffective in preventing pulmonary tuberculosis infection (2). Thus, understanding the intracellular survival mechanisms employed by Mtb is vital to developing new anti-tuberculosis treatments and vaccines.

Macrophages, phagocytic innate immune cells that are generally competent for bacterial killing, represent the primary intracellular niche for Mtb. Some of the antimicrobial mechanisms utilized by macrophages include acidification of the phagosome, production of reactive oxygen and nitrogen species, fusion of lysosomes to bacterial containing phagosomes and autophagy (3-6). However, despite these robust defenses, Mtb survives inside macrophages during its infectious life cycle. To facilitate its survival Mtb has evolved to resist macrophage defenses, either by directly protecting the bacterial cell from damage (7-9) or by modulating the macrophage's ability to shuttle the bacteria through the traditional phagolysosomal maturation process (10). In that way, Mtb prevents its intracellular compartment from acidifying (11) and fusing (12) with the destructive lysosome. Genetic studies have identified several Mtb proteins important for remodeling host membrane trafficking (13-15). For example, Mtb *Rv3310* encodes SapM, a secreted acid phosphatase (16) that converts phosphatidylinositol 3-phosphate (PI3P) to phosphatidylinositol. Loss of PI3P from the phagosome membrane is sufficient

to prevent fusion of phagosomes with late endosomes (17, 18). Importantly, many genes reported to be important for Mtb survival inside macrophages remain uncharacterized (13, 14, 19) and the manipulation of the host cell by Mtb remains poorly understood.

The problem of intracellular survival faced by Mtb is also shared by other bacterial pathogens, and many of these organisms utilize specialized secretion systems to deliver molecules into the host cell to establish a unique intracellular niche (20). For example, some Gram-negative pathogens use needle-like machines that span the bacterial and host cell membranes to inject protein cargo into the host (21-24). Encoded by a Type III Secretion System (TTSS), the needle-like machine shares its structure with the bacterial flagellum and is expressed by a number of intracellular pathogens including *Salmonella enterica* subsp. *enterica* serovar Typhimurium, *Shigella flexneri*, and *Chlamydia trachomatis* (21, 22). Another specialized secretion machine called a Type IV Secretion System is found in Gram-positive and Gram-negative bacteria and can used for translocation of nucleic acid through conjugation (23) while in many human and plant pathogens such as *Legionella pneumophila, Coxiella burnetii* and *Agrobacterium tumefaciens,* it also transports effector proteins that promote bacterial survival (25, 26). The Type VI Secretion System is structurally analogous to the bacteriophage tail spike and is expressed by pathogenic bacteria including *Francisella tularensis, Pseudomonas aeruginosa and Vibrio cholera* (24, 27, 28). Finally, Mtb encodes multiple Type VII secretion systems, discussed below, that are important in pathogenesis (29, 30). However, the identity and functions of the Type VII dependent secreted proteins remain unknown. Despite structural differences, a common theme is

103 that these elaborate secretion systems aid in pathogenesis by delivering virulence
104 proteins called “effectors” to the host cell.
105 Effectors are proteins that promote bacterial survival by manipulating vital cellular
106 processes including signal transduction, vesicular trafficking and the cytoskeleton (31-
107 33). Like the secretion systems themselves, the repertoire of effectors expressed by
108 each pathogen can differ, adapted specifically for each unique life cycle. However, a
109 major common target for effectors are host membranes. For example, SifA from *S.*
110 *typhimurium* is prenylated inside the host cell and localizes to the Salmonella containing
111 vacuole (SCV) (34). SifA recruits lysosomes to maintain SCV membrane integrity and
112 its membrane interaction is vital to Salmonella pathogenicity (34, 35). The *Legionella*
113 *pneumophila* Type IV secreted effector SidM is anchored to the Legionella containing
114 vacuole and disrupts host vesicle trafficking by sequestering and modifying Rab1 (36).
115 Some effectors can also function by directly modifying membranes such as IpgD from
116 *S. flexneri* that hydrolyzes phosphatidylinositol 4,5-bisphosphate (PI(4,5)P_2) to
117 phosphatidylinositol 5-monophosphate (PI5P) leading to membrane blebbing and
118 bacterial uptake into host cells (37). Thus, both host membranes themselves and
119 membrane-dependent processes represent valuable targets for bacterial effectors (31,
120 33, 38) as we recently showed for a variety of bacterial pathogens (39).
121 The virulence functions of most Mtb secreted proteins are poorly understood. Although
122 Mtb does not encode a T3SS, it does contain the conserved general secretion systems
123 Sec and Tat (40), as well as multiple Type VII (also called ESX) secretion systems (30).
124 The ESX-1 system is required for Mtb virulence in macrophages and mouse models of
125 infection (29) through modulation of immune functions such as induction of Type I

126 interferon via the secreted effectors EsxA and EsxB (41, 42). Similarly, EsxH, a
127 substrate of the ESX-3 system, interacts with a component of the host endosomal
128 sorting complex required for transport (ESCRT) machinery, leading to decreased co-
129 localization of Mtb with lysosomes (43) and inhibition of antigen presentation in infected
130 macrophages (44). Substrates of the accessory SecA2 system such as the protein
131 kinase PknG and the esterase LipO are also important for Mtb virulence by contributing
132 to phagosome maturation arrest (PMA) (13, 18, 45, 46). Thus, because membrane
133 processes are high value targets of many bacterial effectors (39, 47), and Mtb has a
134 large repertoire of exported proteins of unknown function (48-52), we hypothesized that
135 some of the Mtb exported proteins are membrane-binding effectors with virulence
136 activities.
137 To test our hypothesis we generated a library of 200 exported proteins from Mtb, tested
138 whether they individually bound yeast membranes in a life or death assay, and
139 characterized their ability to alter host protein secretion in an inducible secretion assay.
140 We also determined the subcellular localization of each membrane-binding protein
141 using fluorescence microscopy. By combining data from the cell biological screens, we
142 identified five Mtb exported proteins that localized to eukaryotic membranes and
143 inhibited protein transport through the host secretory pathway. One protein, Mpt64
144 (Rv1980c), localized to the ER during both heterologous expression in HeLa cells and
145 Mtb infection of macrophages. Though Mpt64 is a Sec substrate, its access to the
146 macrophage cytoplasm was dependent on the ESX-1 secretion system. Finally, bacteria
147 lacking Mpt64 were attenuated for growth in primary human macrophages,
148 demonstrating an important virulence activity for Mpt64.

Results

Categorization of putative effector-like proteins from Mtb

Through the analysis of published datasets we identified Mtb proteins that may function as secreted effectors (Supplemental Table 1). For clarity, we define these proteins as Mycobacterial exported proteins (MEPs), as this encompasses proteins that are secreted as well as those delivered to the mycobacterial surface, which can still modulate interactions with the host (53, 54). We used the following criteria to assemble a library of MEPs: 1) Mtb secreted proteins identified via proteomic approaches (49-52, 55, 56), 2) Mtb proteins known to be involved in manipulation of host vesicular trafficking pathways, such as ones that induce mammalian cell entry (MCE) (57-59) or phagosome maturation arrest (13, 14, 60), 3) a subset of PE/PPE proteins and proteins related to those encoded by Type VII (ESX-1) loci (61-63), and 4) proteins involved in virulence, ranging from defined to unknown functions (19, 54, 64-66). We then used Gateway recombination cloning to subclone MEPs from the freely available Mtb ORFome Gateway compatible library (BEI) into destination vectors for a variety of subsequent assays. The comprehensive list of MEPs is shown in Supplemental Table 1.

Mtb encodes exported proteins that interact with eukaryotic membranes

To identify membrane binding Mtb proteins, we used a system that leverages the signal transduction of the essential yeast GTPase Ras to promote growth and division (67). Ras is lipidated at a unique sequence called the CaaX box that promotes its localization to the plasma membrane, where it can be activated by Cdc25, a guanine nucleotide exchange factor (67, 68). In a yeast strain with a temperature sensitive *CDC25* allele, yeast can only grow at the permissive temperature (25°C) but not the restrictive

temperature (37°C) because Ras activation requires interaction with Cdc25. Heterologous expression of a non-lipidated, constitutively-active Ras whose activity is independent of Cdc25 (Ras^{mut}) can rescue yeast growth at the restrictive temperature when Ras is recruited to intracellular membranes by fusion to a membrane binding protein (Fig. 1A). This system has been used to successfully identify membrane binding effectors from Gram negative pathogens (39). To identify membrane-localizing proteins from Mtb, we subcloned MEPs into a destination vector for yeast expression that generates an in-frame fusion of the MEP to Ras^{mut}. We transformed *S. cerevisiae cdc25*^{ts} (39, 67) individually with each of the 200 MEP fused to Ras^{mut} and incubated them at both permissive and restrictive temperatures (Figure 1B). We identified 52 Mtb proteins that rescued *S. cerevisiae cdc25*^{ts} growth at the restrictive temperature (Fig. 1B, C).

We confirmed expression of the Ras^{mut}-MEP fusion proteins by Western blotting (Figure 1D). In addition, we determined the membrane localization of each MEP by fluorescence microscopy of GFP-MEP fusion proteins in yeast (Fig. 1E). It has been established that Ras can function from membranes other than the plasma membrane (69, 70) and Ras^{mut} maintains this function (39). Thus, using fluorescence microscopy we observed GFP-MEP fusion proteins localizing to distinct subcellular compartments including vacuoles, ER and plasma membrane (Figure 1E). Together these results show that 25% of the MEPs tested could associate with the membranes of a variety of organelles in *S. cerevisiae*.

Subcellular localization of membrane-localizing MEPs

While many cellular processes are conserved in eukaryotes, humans represent the primary natural host for Mtb. Therefore, to confirm that MEPs that rescued *S. cerevisiae cdc25*^{ts} growth at 37°C also bound mammalian membranes and to determine their subcellular localization in human cells, we transiently transfected HeLa cells with vectors for constitutive expression of GFP-MEP fusion proteins and then used fluorescence microscopy with co-localization markers to identify the specific membrane to which each MEP localized (Figure 2A). We identified GFP-MEP fusion proteins that localized to a variety of subcellular compartments including the ER, Golgi, mitochondria and peroxisomes (Figure 2A and 2B). The largest proportion of the GFP-MEP fusion proteins expressed in human cells co-localized with the ER marker calreticulin (Figure 2B). In yeast, we observed a similar number of GFP-Mtb fusion proteins which localized to compact, punctate structures (data not shown). Although there was only moderate overlap in the subcellular localization identified between yeast and HeLa cells (Figure 2B), we were able to verify that the proteins identified by the Ras rescue assay are localized to membranes in human cells.

A subset of mycobacterial exported proteins alter the host secretory pathway

Membrane-bound cargo is transported within the host cell and to the extracellular space in dynamic vesicular trafficking pathways. The membrane-bound and soluble proteins important for these processes are frequent targets of bacterial effectors (47, 71). Indeed, Mtb is known to target and manipulate trafficking pathways through incompletely understood mechanisms (43, 72, 73). To determine if Mtb proteins can broadly affect the host general secretion pathway as an indicator of interaction with membranes and intracellular vesicular trafficking, we took advantage of the reverse

dimerization system (74). In this system, a secreted protein of interest is sequestered in the ER by fusion to a conditional aggregation domain (CAD). Addition of a solubilization molecule that disrupts the CAD then frees the fusion protein for trafficking and secretion into the extracellular space. We used a fusion of human growth hormone (hGH) to the CAD domain of the ligand-reversible crosslinking protein, FKBP F36M. Thus, hGH can be quantified in cell supernatants by ELISA after addition of the small molecular, D/D Solubilizer (Figure 3A) (74, 75). We transfected HeLa cells expressing hGH-CAD with each MEP individually, a negative control protein (GFP), or an enterohemorrhagic *Escherichia coli* effector (EspG) that inhibits secretion by promoting the tethering of vesicles to the Golgi apparatus (75, 76). When we treated transfected cells with D/D Solubilizer, we observed a spectrum of effects on the secretion of hGH including increased, decreased and normal hGH secretion (Figure 3B and Supplemental Table 1). Using a cut-off of normalized hGH secretion below 0.25 or above 1.75, we identified 10 proteins that decreased hGH secretion and 10 proteins that increased hGH secretion as compared to the GFP control (Figure 3C). We next compared the MEPs that altered host secretion to those that bound eukaryotic membranes, and identified five proteins with overlapping activities: Rv0594, Rv1646, Rv1810, Rv1980c and Rv2075 (Figure 3D). During expression in HeLa cells, all but one protein localized to the ER and all five proteins reduced hGH secretion (Figure 3E).

Mpt64 N-terminus is important for membrane binding and secretion inhibition

We focused on the protein Rv1980c, also known as Mpt64, as it is a secreted protein that is highly antigenic during human tuberculosis infection (77, 78). Furthermore, Mpt64 is a component of the region of difference 2 (RD2) locus, one of the genomic regions

240 deleted during attenuation of the *M. bovis* BCG vaccine strain (79). Loss of RD2 from
241 Mtb attenuates its virulence, and complementation with a three gene cluster that
242 includes Mpt64 can partially restore virulence (80).

243 Mpt64 is a 25kDa protein with a predicted signal peptidase 1 cleavage site
244 between amino acids 23 and 24, such that the mature, secreted form of the protein
245 starts at amino acid 24 (50, 51, 81). While the solution structure of Mpt64 was
246 previously solved (82), the structure does not align to a known catalytic domain but
247 does contain a domain of unknown function (DUF3298). This domain is also present in
248 the lysozyme-binding anti sigma factor RsiV (83). Despite structural homology between
249 Mpt64 and RsiV (Supplemental Figure 1A) (84), there is little primary sequence
250 homology. To determine if Mpt64 binds lysoszyme, we purified recombinant Mpt64 from
251 *E. coli* and tested binding to human or hen egg white lysozyme in an *in vitro* pull down
252 assay (83). Using this assay we were unable to demonstrate lysozyme binding by
253 Mpt64 (Supplemental Figure 1B). We next used the solution structure to guide
254 truncation analysis of Mpt64 in order to identify the membrane binding sequences of
255 Mpt64 (Figure 4A and Figure 4B). *S. cerevisiae cdc25*^{ts} expressing a fusion of Ras^{mut}
256 with either full length Mpt64, mature Mpt64 lacking its predicted signal peptide or the N-
257 terminal half of Mpt64 also lacking the signal peptide (Mpt64_24-143) were able to grow
258 at 37°C, whereas *S. cerevisiae cdc25*^{ts} expressing Ras^{mut} fused to the C-terminal half of
259 Mpt64 (Mpt64_144-228) could not (Figure 4C). We detected expression of Ras^{mut}
260 fusions of full length Mpt64 and mature Mpt64 by Western blot. In contrast, we could not
261 detect Ras^{mut} fusions of Mpt64_24-143 or Mpt64_144-228 despite the fact that the
262 Mpt64_24-143 fusion rescued yeast growth, suggesting that expression of Mpt64_24-

263 143 below the limit of detection by Western blot was still sufficient to rescue yeast
264 growth (Figure 4D). However, whether the C-terminal domain plays a role in membrane
265 binding could not be determined definitively because we were unable to demonstrate
266 stable fusion protein expression. To test if Mpt64 could interact with lipids directly, we
267 expressed and purified recombinant Mpt64 and Mpt64 variants from *E. coli* and tested
268 their ability to bind unique lipid species i*n vitro* using membranes spotted with lipids.
269 Recombinant Mpt64_24-228 bound phosphatidylinositol 4-phosphate (PI4P),
270 phosphatidylinositol 5-phosphate (PI5P), phosphatidylinositol 4,5-bisphosphate
271 [PI(4,5)P_2] and phosphatidylinositol (3,4,5)-trisphosphate [PI(3,4,5)P_3] on PIP strips
272 membranes (Figure 4E). Similarly, recombinant Mpt64_24-143, the N-terminal portion of
273 the protein, also bound PI4P and PI5P with additional binding to PI3P, PI(3,4)P_2 and
274 phosphatidylserine (Figure 4E). However, interaction with PI(4,5)P_2 and PI(3,4,5)P_3 was
275 weak, suggesting that the C-terminal region of Mpt64 modifies its interactions with host
276 phospholipids.

277 Finally, we sought to determine if the N-terminal portion of Mpt64 was also
278 sufficient to inhibit hGH secretion using the hGH-CAD assay. We co-transfected hGH-
279 CAD expressing HeLa cells with the same Mpt64 truncations and determined their
280 ability to inhibit hGH secretion in the presence of drug. Similar to the Ras rescue assay,
281 full length, mature and Mpt64_24-143 inhibited hGH secretion compared to the GFP
282 control. In contrast, co-transfection of Mpt64_144-228 with hGH-CAD had no effect on
283 its secretion (Figure 4F). These data suggest that the ability of Mpt64 to bind
284 membranes and to inhibit host secretion *in vitro* is dependent on the N-terminus of the
285 protein.

Mpt64 ER localization depends on its N-terminus

As full-length Mpt64 localized to the ER in yeast and HeLa cells (Fig. 1,3) we next tested the impact of Mpt64 truncations on ER localization. We first determined the phenotypic localization of Mpt64 truncations expressed as GFP fusions in yeast using fluorescence microscopy. Mpt64_1-228 and Mpt64_24-228 localized in a ring indicative of the ER (85, 86)(Figure 5A). In contrast Mpt64_144-228, which did not rescue yeast growth in the Ras Rescue assay (Figure 4C), was diffuse throughout the yeast cell (Figure 5A). Interestingly, Mpt64_24-143 localized to bright puncta within the cells (Figure 5A). To confirm the N-terminal dependence of Mpt64 localization, we transfected HeLa cells with GFP fusions to each Mpt64 truncation and assayed for co-localization with calreticulin through immunofluorescence microscopy. While full length Mpt64, mature Mp64 and Mpt64_24-143 co-localized with calreticulin, Mpt64_144-228 did not (Figure 5B). These results demonstrate that Mpt64 localizes to the ER during exogenous expression in both yeast and mammalian cells and the N-terminal 143 amino acids are sufficient for Mpt64 to localize to membranes.

Secreted Mpt64 localizes to the ER during infection

Although we observed Mpt64 localization to the ER in yeast (Figure 1E and Figure 5A) and HeLa cells (Figure 5B), we wanted to determine if endogenous, untagged Mpt64 localizes to the ER during an Mtb infection of macrophages. To that end, we infected mouse RAW267.4 macrophages with mCherry-labeled Mtb at an MOI of 20:1 and fixed cells at various time points after infection. We then used a rabbit polyclonal antibody developed against recombinant, mature Mpt64 protein to track Mpt64 secretion from Mtb into macrophages using immunofluorescence microscopy. Of

309 note, this antibody was generated without complete Freund's adjuvant in order to avoid
310 any cross-reactivity against Mtb antigens generated by the use of this adjuvant. As little
311 as four hours after infection, endogenous Mpt64 was detected in both the cytoplasm
312 and ER of host cells (Figure 6A, upper panels). When we performed the same
313 experiment with MtbΔeccD1, a strain that lacks the Type VII secretion system secretion
314 pore that cannot secret ESAT-6 (29, 87, 88) and does not result in communication
315 between the phagosome and cytoplasm (41, 42, 89), Mpt64 appeared to be secreted
316 but trapped adjacent to the bacteria (Figure 6A, lower panels), suggesting that it could
317 not escape the phagosome. Importantly, Mpt64 was detected in the culture filtrate
318 prepared from MtbΔeccD1 (Supplemental Figure 2A). Thus, although Mpt64 is likely
319 secreted from Mtb by the canonical Sec-dependent pathway, its access to the
320 macrophage cytoplasm and other targets in the cell was dependent on the Type VII
321 secretion system.

322 In order to better understand the role of Mpt64 in Mtb virulence, we used
323 mycobacteriophage (90-92) to introduce the hygromycin resistance cassette into the
324 *Mpt64* gene to create an in-frame deletion (Figure 6B). We confirmed disruption of
325 *Mpt64* by PCR (Supplemental Figure 2B) and loss of Mpt64 by the absence of protein
326 on Western blot (Figure 6C). We then complemented MtbΔMpt64 with either full length
327 Mpt64 (MtbΔMpt64::Mpt64) or Mpt64 lacking its signal peptide (MtbΔMpt64::Mpt64-NS)
328 under the control of the constitutive mycobacterial strong promoter (93). Both
329 complemented strains expressed Mpt64 but only full-length Mpt64 (MtbΔMpt64::Mpt64)
330 could be detected in the supernatant of cultures, confirming that deletion of the signal
331 peptide inhibits Mpt64 secretion from Mtb (Figure 6C). Furthermore, the

MtbΔMpt64::Mpt64 strain had modestly higher expression of Mpt64 compared to wild-type Mtb by western blot, consistent with our use of a strong constitutive promoter for complementation. All four strains grew equally under axenic growth conditions (Supplemental Figure 2C), and we confirmed that both Mtb and MtbΔMpt64 produced phthiocerol dimycocerosate by mass spectrometry (Supplemental Figure 2D).

To test if secreted Mpt64 interacts with the ER during infection, we assessed its colocalization with calreticulin in RAW267.4 cells using confocal immunofluorescence microscopy. When we infected RAW267.4 macrophages, the Mpt64 signal in Mtb infected macrophages co-localized with calreticulin, confirming the subcellular localization of Mpt64 secreted during infection (Figure 6D,E and Supplemental Figure 3). However this co-localization was lost in cells infected with MtbΔMpt64::Mpt64-NS bacteria (Figure 6D,F and Supplemental Figure 3). As a control for antibody specificity, no Mpt64 was detected in macrophages infected with MtbΔMpt64 mutant bacteria (Figure 6D and Supplemental Figure 3). From these data, we can confirm that the signal peptide of Mpt64 is sufficient for the protein's secretion in vivo and is required (with concerted action of the Type VII secretion system) for Mpt64 to interact with the ER during infection.

Mpt64 contributes to early Mtb growth after aerosol infection of mice.

Because Mpt64 is part of the Mtb RD2 locus that partially accounts for the attenuation of Mtb (80), and our data indicating that Mpt64 may function as a secreted effector, we investigated the role of Mpt64 in Mtb virulence in a murine model of infection. We infected BALB/c mice via aerosol with a low-dose of bacteria (~100 CFU Mtb) and collected lungs at various time points to determine CFU and histopathology. We

compared the infections of four strains: wild type Mtb, MtbΔMpt64, MtbΔMpt64::Mpt64 and MtbΔMpt64::Mpt64-NS (described in Figure 6). While all mice received equal numbers of bacteria between the four strains at day 0 (data not shown), there were fewer Mtb isolated from lungs of mice infected with the MtbΔMpt64 mutant compared to wild type (mean CFU wild type Mtb $2.7x10^6$ vs MtbΔMpt64 $1.7x10^6$, p=0.07) at 21 days post infection (dpi) but no statistically significant difference by 42dpi (mean CFU wild type Mtb $5.0x10^5$ vs MtbΔMpt64 $3.4x10^5$). However, by 42dpi there was a statistically significant decrease in the CFU isolated from lungs of mice infected with MtbΔMpt64::Mpt64-NS (Figure 7A). At these time points, we observed a reduction in the area of inflammation in hematoxylin and eosin (H&E) stained lungs of mice infected with MtbΔMpt64::Mpt64-NS compared to wild type. (Figure 7B and 7D). Despite modest reductions in CFU in mutant bacteria, there were no differences in mouse survival comparing the four strains (Figure 7C). Thus, although deletion of *Mpt64* entirely (MtbΔMpt64) and disruption of Mpt64 secretion (MtbΔMpt64::Mpt64-NS) resulted in a modest decrease in bacterial growth in the lungs of mice, loss of Mpt64 was not sufficient to explain the attenuation of the RD2 mutant (80).

Mtb survival in human macrophages requires Mpt64

Next, we assessed whether the localization of Mpt64 in human cells is similar to that in murine macrophages. To that end, we infected primary human monocyte-derived macrophages with mCherry-expressing WT Mtb or MtbΔeccD1 and stained for Mpt64. Consistent with our data in RAW267.4 cells (Figure 6A) the secretion of Mpt64 to extra-phagosomal sites in primary human macrophages was dependent on the Type VII Secretion System (Figure 8A). Then we infected primary human macrophages with WT

Mtb, MtbΔMpt64, MtbΔMpt64::Mpt64 or MtbΔMpt64::Mpt64-NS and determined the co-localization of Mpt64 with calreticulin by fluorescence microscopy (Figure 8B and Supplemental Figure 4). At 4hpi, we detected co-localization of Mpt64 with calreticulin in cells infected with WT Mtb and MtbΔMpt64::Mpt64 (top panels) but not in cells infected with MtbΔMpt64 or MtbΔMpt64::Mpt64-NS (bottom panels, Figure 8B).

To better understand the contribution of Mpt64 in the context of human Mtb infection, we determined the growth of wild type, MtbΔMpt64 or MtbΔMpt64::Mpt64 in primary monocyte-derived human macrophages. We recovered CFU from cells directly after infection (Day 0) and one and three days post infection. While there was no difference in the CFU isolated from cells infected with each strain after one day of infection, the MtbΔMpt64 mutant was attenuated for growth three days post infection compared to wild type (Figure 8C). This growth defect was rescued in the complemented strain. Together these data indicate a role for Mpt64 in the virulence of Mtb during acute infection of human macrophages.

Discussion

Numerous efforts have been undertaken to identify Mtb exported proteins, from lipoproteins that are incorporated into the cell wall, to virulence factors that reach the extracellular environment such as ESAT-6 (48-50). However, little is known about the function of this “secretome” as a whole. Here we took a systematic approach towards characterizing host-dependent interactions of a collated list of putative effector molecules. We created a library of 200 putative mycobacterial exported proteins and then through a series of cell biological screens characterized these MEPs for their ability to bind eukaryotic membranes, their subcellular localization and their ability to modulate

401 secretion of a model substrate. In addition, we demonstrate that one secreted protein,
402 Mpt64, localized to the ER during infection and was important for virulence of Mtb in
403 human macrophages. The cohort of 200 MEPs we generated was large but not
404 necessarily exhaustive (Supplemental Table 1). For example, the 76 PE/PPE genes we
405 included represent less than half (45%) of the total number of PE/PPE genes in the Mtb
406 genome (94). In addition, a recent technology called EXIT identified 593 Mtb proteins
407 secreted during intravenous infection of mice including 38 proteins that are significantly
408 enriched only during *in vivo* infection as compared to growth on 7H10 agar, suggesting
409 a virulence function for these proteins (95). Of the 200 MEPs we characterized, 51
410 overlap with those identified by EXIT and of the 51 overlapping proteins, 25 are
411 membrane associated in our study. This emphasizes that host membranes can be
412 targets of Mtb virulence proteins.

413 We found 52 Mtb proteins that associated with eukaryotic membranes,
414 representing nearly 25% of the total screened. When the membrane association of type
415 III and type IV effectors from several Gram negative pathogens was explored, about
416 30% of effectors screened also associated with eukaryotic membranes (39). While our
417 data are in agreement with this value, pathogens that replicate intracellularly in vacuoles
418 had even higher numbers of membrane-associated effectors (39). This suggests that
419 there may be additional secreted virulence proteins from Mtb that associate with the
420 host membranes than our screen identified. Indeed, while we corroborated previously
421 known membrane-interacting proteins such as the SecA2-secreted PI3P phosphatase
422 SapM (17, 18), the Rac1-binding protein Ndk (96) and the cholesterol-binding Mce4A
423 (97), we failed to identify others such as LipY which hydrolyzes extracellular lipids (98)

424 and the ESX1 substrate ESAT-6 which interacts with the phagosomal membrane (99,
425 100).

426 GFP-Mpt64 localized to the ER in both yeast and mammalian cells. Additionally,
427 endogenous Mpt64 localized to the ER during Mtb infection of macrophages,
428 suggesting that the observed localization of Mpt64 is not an artifact of heterologous
429 over-expression. Mpt64 did not co-localize with the ER after infection with a Type VII
430 secretion system mutant underscoring the importance of the membrane disrupting
431 properties of ESAT-6 in establishing communication with the host cell (99, 100). This
432 ESX-1 dependent mechanism of cytoplasmic access is similar to the route taken by the
433 autotransporter-like protein tuberculosis necrotizing toxin (TNT) (101, 102). Thus, our
434 data strengthen the argument that the Type VII secretion system facilitates access of
435 non-ESX-1 substrates beyond the phagosome and into the host cell.

436 We identified PI4P and PI5P as primary monophosphotidylinositol targets of
437 recombinant Mpt64, in addition to the di- and tri-phosphotidylinositols PI(4,5)P_2 and
438 PI(3,4,5)P_3. While PI4P is thought to be enriched in the Golgi (103), it also has an
439 established role in mediating protein trafficking from ER exit sites (104, 105). Thus, the
440 ability of Mpt64 to block secretion may stem from its subcellular localization at the ER,
441 interaction with PI4P, and interference with ER to Golgi trafficking. Less is known about
442 PI5P as its basal level is only about 1% of PI4P (106). However, PI5P is increased
443 during bacterial infection and other stresses, and can be found throughout the cell,
444 including the ER (106). Likewise, while PI(4,5)P_2, the most abundant
445 phosphotidylinositol, is distributed predominantly at the plasma membrane, it can also
446 be found within the cell at the Golgi and ER (107), and PI(4,5)P_2 serves as the

447 precursor for cellular production of PI(3,4,5)P_3 (108). Taken together, while Mpt64 binds
448 multiple phosphotidylinositols in vitro, the relative contributions of binding to individual
449 molecules and the role of such binding in mediating the host secretion blockade of
450 Mpt64 remain unknown.

451 Disruption of the RD2 locus in Mtb H37Rv leads to decreased bacterial burdens
452 in the lungs and spleen of aerosol-infected mice at 3 weeks after infection (80). As
453 Mpt64 is within the RD2 locus, we hypothesized that the single, in-frame deletion of
454 Mpt64 might explain the attenuation phenotype of the RD2 mutant. In line with this
455 prediction, we observed decreased bacterial burdens of MtbΔMpt64 compared to WT
456 Mtb in the lungs of mice at 3 weeks post-infection. Although this decrease was not
457 statistically significant and was not associated with a survival defect, it does suggest
458 Mpt64 contributes to the virulence of the RD2 region. Other genes located in the RD2
459 locus that were not complemented in the RD2 survival study (80) such PE_PGRS35
460 (Rv1983) and cfp21 (Rv1984) may also contribute alongside Mpt64 to the virulence
461 defect observed in RD2 deletions. Furthermore, it is possible that one or more of the
462 other Mtb secreted proteins we identified, including the 27 proteins that also localize to
463 the ER are able to perform a redundant function to that of Mpt64 during an animal
464 infection. In a similar vein, whereas *L. pneumophila* encodes over 300 effectors,
465 individual *L. pneumophila* effector deletion mutants are not defective for growth in cells
466 or mice (109, 110). Thus, future work disrupting multiple Mtb MEPs simultaneously will
467 help address the issue of redundancy.

468 When we infected mice with MtbΔMpt64::Mpt64-NS, a strain of Mtb that still
469 expresses Mpt64 but cannot secrete it into the host cell, we recovered significantly

470 fewer CFU compared to WT from the lungs of MtbΔMpt64::Mpt64-NS infected mice. We
471 hypothesize that this strain suffers from two detrimental consequences. First, blocking
472 Mpt64 secretion prevents it from exerting its virulence function in the host. Second, non-
473 secreted Mpt64 can still be cross-presented to the adaptive immune system (111), thus
474 leading to a cell mediated immune response against Mpt64. This observation is
475 consistent with data that both human patients with active tuberculosis and their PPD
476 positive contacts have T-cell responses to Mpt64 (112) and T-cell reactive Mpt64
477 epitopes have been mapped (113). Furthermore, Mpt64 staining is observed in
478 granulomas of infected individuals (114, 115). Thus, Mpt64 is highly immunogenic
479 during human infection with Mtb and suggests an evolutionary tradeoff between the
480 virulence function of Mpt64 and its antigenicity. In fact, when we explored the
481 importance of Mpt64 in human disease, we observed that Mpt64 secreted from wild
482 type bacteria localized to the ER of infected human monocyte-derived macrophages
483 and its presence enhanced the survival of Mtb within primary human macrophages.
484 Together these findings suggest that Mpt64 contributes to the virulence of Mtb in human
485 disease.

Materials and Methods

Bacterial Strains and Growth Conditions

M. tuberculosis Erdman and mutants were grown in Middlebrook 7H9 broth or on Middlebrook 7H11 agar (Difco) supplemented with 10% oleic acid-albumin-dextrose-catalase (OADC, Remel). Liquid medium was also supplemented with 0.05% Tween 80.

Yeast Strains and Assays

The *Saccharomyces cerevisiae* strain INVSc1 (Invitrogen) was grown at 30°C in histidine drop out media (SD/-HIS) or agar plates (Clontech). The construction of cdc25^{ts} was previously described (68). cdc25^{ts} was grown at 25°C in leucine drop out media or agar plates (SD/-LEU) (Clontech).

The cdc25^{ts} strain and INVSc1 strain were transformed using a lithium acetate (LiAc) protocol. Yeast were grown to high density overnight at the appropriate temperature, shaking. The cultures were diluted to an OD_{600}=0.2 in 50mL YPD and allowed to reach mid-log phase. Cells were washed, resuspended in 0.1M LiAc and incubated 10 minutes at room temperature. The sample DNA was mixed with an equal volume of pre-boiled Yeastmaker Carrier DNA (Clontech). To the DNA was added 100uL yeast and 500uL of a solution of LiAc+PEG (40% PEG w/v, 0.1M LiAc). This solution was incubated 30 minutes at 25°C (cdc25^{ts}) or 30°C (INVSc1) with agitation every 10 minutes. DMSO was added and the cells were heat shocked at 42°C for 15 minutes. The cells were pelleted, washed in TE and resuspended in 500uL TE. The transformed cells were plated on selective agar plates and incubated at the appropriate temperature for 2-4 days.

509 To perform the Ras rescue assay, 3-4 fresh colonies were combined in 30μL
510 SD/-LEU and 3 μl was spotted onto duplicate plates that were subsequently incubated
511 at either 25°C or at 37°C for 2 days.
512 INVSc1 yeast were transformed with a galactose-inducible vector
513 (p413GALGFP) containing GFP-Mtb fusion proteins and selected on SD/-HIS. To
514 induce protein expression, yeast were inoculated in 3mL galactose/raffinose (Gal/Raf)
515 base lacking histidine (Clontech) and allowed to grow 16-20 hours at 30°C, shaking.
516 Cultures were pelleted, resuspended in 30-50uL PBS and immobilized on an agar pad
517 prior to visualization.
518
519 Yeast Lysis and Western Blotting
520 Yeast (cdc25^{ts}) were inoculated into 5mL SD/-Leu and incubated overnight at room
521 temperature, shaking (250rpm). To lyse, 1.5mL of each culture was centrifuged at
522 14,000rpm for one minute. Each pellet was resuspended in 100μL 2.0M LiAc and
523 incubated on ice for five minutes. Samples were centrifuged at 14,000 for one minute to
524 pellet, resuspended in 100μL 0.4M NaOH and incubated on ice for five minutes.
525 Samples were pelleted as before, resuspended in 75μL 1x SDS Laemmli sample buffer
526 and boiled at 100°C for five minutes. Lysates were centrifuged 14,000rpm for one
527 minute to remove to debris, separated by SDS- polyacrylamide gel electrophoresis and
528 transferred to polyvinylidene difluoride membrane for Western blotting. Fusion proteins
529 were detected by rabbit anti-Ras (1:100) and equal loading was confirmed by detection
530 with rabbit anti-G6PDH (1:10,000).
531

532 Cell Culture

533 HeLa cells were cultured in Dulbecco's modified Eagle medium (DMEM, Gibco)
534 supplemented with 10% fetal bovine serum (FBS, Gibco), 100 I.U./mL penicillin, 100
535 µg/mL streptomycin, 292 µg/mL L-glutamine (Corning). RAW267.4 macrophages were
536 cultured in RPMI 1640 (Gibco) supplemented with 10% heat-inactivated FBS, 100
537 I.U./mL penicillin, 100 µg/mL streptomycin, 292 µg/mL L-glutamine, and 10mM HEPES
538 (Hyclone).

539 Primary human macrophages were isolated from buffy coats from anonymous
540 donors provided by a local blood bank. To isolate, 50mL of blood from each donor was
541 added to an equal volume of PBS then separated by centrifugation over a Ficoll-Paque
542 Plus gradient at 750 x g for 20 minutes with no brake. The lymphocyte/monocyte layer
543 was collected and incubated 1-2 minutes with 1mL ACK lysing buffer (Gibco) to remove
544 red blood cells. The cells were diluted to 50mL in PBS and centrifuged 350 x g for 10
545 minutes at 4°C. The supernatant was removed and cells were washed in 25mL PBS
546 and pelleted at 160 x g for 15 minutes at 4°C. Cells were washed again in 25 mL PBS
547 but centrifuged at 300 x g for 10 minutes at 4°C. This final pellet was resuspended in 5-
548 10 mL of RPMI 1640 supplemented with 10% human AB serum (Corning). To
549 differentiate into macrophages, cells were cultured in RPMI 1640 supplemented with
550 10% human AB serum and 50ng/mL human M-CSF (R&D Systems) for at least 4 hours,
551 washed in PBS then replaced with RPMI 1640 +10% human AB serum + human M-CSF
552 (50ng/mL) for 7 days with media changes every 1-2 days.

553

554 Antibodies

555 To generate an antibody against native Mpt64, two rabbits were immunized with
556 recombinant 6xHIS-tagged Mpt64ΔSP purified from *E. coli* in incomplete Freund's
557 adjuvant (Pacific Biosciences). The polyclonal rabbit antibody to Antigen 85 and
558 mouse anti-GroEL2 (CS-44) are from BEI Resources. Chicken, mouse and rabbit anti-
559 calreticulin were purchased from Abcam and anti-GM130 was purchased from BD
560 Biosciences. Mouse anti-Tom20 F-10 was purchased from Santa Cruz. Rabbit anti-Ras
561 and rabbit anti-glucose-6-phosphate dehydrogenase (G6PDH) were purchased from
562 Cell Signaling Technology and Sigma, respectively. Mouse anti-PMP70 and horse
563 radish peroxidase (HRP)-conjugated secondary antibodies were purchased from
564 Thermo Scientific. Alexa fluor-conjugated secondary antibodies were from Life
565 Technologies.
566
567 Molecular Biology
568 Unless otherwise stated, all Mtb proteins were cloned from the BEI resources Gateway
569 Mtb ORF library using Gateway cloning technology (Life Technologies). The Mpt64
570 truncation mutants were PCR amplified (Supplemental Table 2) and cloned into pENTR
571 (Life Technologies) prior to cloning into subsequent destination vectors.
572
573 hGH Secretion Assay and Quantification
574 HeLa cells were plated in 24-well plates to achieve approximately 50,000 cells/well 24h
575 prior to transfection. Cells were co-transfected with 1 µg hGH-CAD and 1µg GFP-Mtb
576 effector or GFP alone using FuGene 6 (Promega) per manufacturer instructions. Cells
577 were transfected 16-18h at 37°C 5% CO_2. The transfection media was then aspirated

578 and replaced with DMEM containing 2 μM D/D Solubilizer (Clontech) and incubated for
579 2 h at 37°C 5% CO_2. The plates were centrifuged at 1500 RPM for 5 minutes to pellet
580 debris and the culture supernatants were saved at -80°C prior to hGH quantification.
581 Secreted hGH was quantified by ELISA (Roche, 11585878001). Briefly, samples
582 were thawed on ice and 20 μL was transferred to each well containing 180μL sample
583 buffer (1:10). The plate was incubated 1h at 37°C, washed 5 times in 250μL wash buffer
584 and incubated 1h at 37°C with a polyclonal antibody to hGH conjugated to digoxigenin
585 (α-hGH-DIG). The plate was washed as described and incubated 1 h at 37°C with a
586 polyclonal antibody to digoxigenin conjugated to peroxidase (α-DIG-POD). The plate
587 was washed and developed in peroxidase substrate (2,2'-Azinobis [3-
588 ethylbenzothiazoline-6-sulfonic acid]-diammonium salt). The absorbance was read on a
589 Biotek plate reader at 405nm.
590
591 PIP strips membrane binding
592 6xHIS-Mpt64_24-228 and 6xHIS-Mpt64_24-143 were purified by cobalt TALON affinity
593 resin (Clontech). PIP strips (Invitrogen) were blocked for one hour at room temperature
594 in 3% fatty-acid free bovine serum albumin (BSA) in TBST. Mpt64_24-228 or Mpt64_24-
595 143 was diluted to 1.5ug/mL in 3mL 3% fatty-acid free BSA and incubated with the PIP
596 strips for 3h at room temperature with agitation. Membranes were washed three times in
597 3% fatty-acid free BSA prior to incubation with anti-Mpt64 or pre-immune serum
598 (1:3,000) overnight at 4°C, with agitation. Membranes were washed three times in 3%
599 fatty-acid free BSA then incubated with HRP-conjugated donkey anti-rabbit (1:2000) for

600 30 minutes at room temperature. Membranes were washed three times before detection
601 of Mpt64 lipid interactions by chemiluminescence.
602
603 Transfection and co-localzation of MEPs in HeLa cells
604 HeLa cells were transfected overnight with GFP fusion proteins using FuGene 6
605 transfection reagent (Roche). Cells were fixed in 4% paraformaldehyde (PFA) for 15
606 minutes, washed in PBS and permeabilized in 0.25% Triton X-100 for 3 minutes at room
607 temperature or in 100% methanol for 10 minutes at -20°C when using Tom20 antibody.
608 Cells were stained with organelle-specific antibodies for 1h at room temperature.
609 Antibodies were visualized by secondary antibodies conjugated to Alexa Fluor 594.
610 Cells were mounted in ProLong Gold + DAPI and z-stacks were collected on an
611 AxioImager M2 microscope (Zeiss).
612
613 Infection and co-localization of Mpt64 in macrophages
614 Bacteria were washed repeatedly in PBS, then sonicated to create a single cell
615 suspension. RAW267.4 cells were infected in DMEM+10% horse serum at MOI 20:1
616 with mycobacteria expressing mCherry. Cells were centrifuged at 1500 rpm for 10
617 minutes to permit bacterial attachment, then allowed to phagocytose for 1.5h at 37°C
618 5% CO_2. Cells were fixed after 4 and 24 hours post-infection in 4% PFA for 60 mintues
619 Cells were permeablized in 0.25% Triton X-100 for 3 minutes at room temperature then
620 blocked in 5% normal donkey serum (Sigma). Mpt64 was detected with rabbit anti-
621 Mpt64 antibody (1:500) and an HRP-conjugated goat-anti rabbit secondary antibody
622 (1:1000, Santa Cruz). Antibody signal was amplified by addition of biotinylated Tyramide

623 (1:50, PerkinElmer) with detection by Alexa fluor 488-conjugated streptavidin (1:250,
624 Jackson Immunoresearch) or Cyanine 5 Tyramide (1:50, PerkinElmer) . Z-stack slices
625 were acquired with an AxioImager M2 microscope (Zeiss).

626 Primary human macrophages were infected in RPMI + 10% human AB serum at
627 an MOI 10:1 with mycobacteria expressing mCherry for 2h at 37°C 5% CO_2 to allow for
628 phagocytosis. Cells were washed and fixed at 4 hours post-infection in 4% PFA for 45-
629 60 minutes. Cells were permeabilized in 100% ice cold methanol for 10 minutes at -
630 20°C and blocked in 5% normal goat serum (Sigma). Mpt64 was detected with rabbit
631 anti-Mpt64 antibody (1:500) and an HRP-conjugated donkey-anti rabbit secondary
632 antibody (1:500, Thermo Scientific) followed by amplification with cyanine 5 Tyramide
633 (1:50, PerkinElmer). Co-localization of Mpt64 with the ER was detected with chicken
634 anti-calreticulin (1:100), followed by goat anti-chicken-488 (Abcam).

635

636 Macrophage infections for CFU

637 Primary human macrophages were seeded in low-evaporation 24-well plates at
638 approximately 5 $x10^5$ cells/well. Bacteria were washed repeatedly in PBS, then
639 sonicated to create a single cell suspension. Macrophages were infected in RPMI +
640 10% human AB serum at MOI 0.5 for 2 hours at 37°C 5% CO_2 to allow phagocytosis to
641 occur. The cells were washed in PBS then replaced with RPMI + 10% human AB serum
642 and cells were washed every day between time points. The cells were lysed at time
643 zero and subsequent time points in 500 µL 0.5% Triton X-100 in PBS. Serial dilutions
644 were plated on 7H11 plates and colonies were enumerated after 2-3 weeks.

645

646 Construction of the Mtb Mpt64 deletion mutant and complementation

647 An in-frame Mpt64 deletion in Mtb was made using mycobacteriophage as previously
648 described (92). Briefly, 500-bp 5' to the Mpt64 start codon and 500-bp 3' to the Mpt64
649 stop codon were amplified from Erdman genomic DNA (Supplemental Table 2) and
650 sequentially cloned into the multiple cloning sites of pMSG360HYG. This vector was
651 linearized with AflII and DraI and transformed into EL350/phAE87 *E. coli* by
652 electroporation. Phagemid DNA was isolated from pooled colonies and transformed into
653 *M. smegmatis* by electroporation. Plaques were isolated and pooled from *M. smegmatis*
654 lawns and high titer phage was produced. Log phase Mtb Erdman was transduced with
655 phage at 42°C for 4h. Mutants were selected on 7H11+Hygromycin (100µg/mL). Wild-
656 type Mpt64 and Mpt64 lacking its secretion signal were cloned into an integrating vector
657 containing a constitutive promoter (pMV306_MSP), conferring zeocin resistance. The
658 MtbΔMpt64 was transformed by electroporation and complements were selected on
659 7H11 + zeocin (25 µg /mL).

660 To confirm expression and secretion of Mpt64 complements, Mtb strains were
661 grown to late-log phase and pelleted by centrifugation. The culture supernatants were
662 saved and passed twice through 0.22 µm filters. Bacterial pellets were boiled 30
663 minutes in lysis buffer (50mM Tris, pH 7.4, 150mM NaCl) supplemented with Complete
664 Mini protease inhibitor (Roche), then subjected to bead beating to lyse the cells. Protein
665 content in lysates was determined by Bradford assay. Mpt64 expression in the lysates
666 and culture supernatants was detected by Western blotting using a rabbit polyclonal
667 antibody to Mpt64 (1:10,000). Equal loading of samples in the lysates and supernatants

668 was confirmed by Western blotting with anti-GroEL2 (1:500) and anti-antigen 85
669 (1:1000) respectively.
670
671 Mouse infections
672 Female BALBc mice (The Jackson Laboratory) were infected via aerosol as described
673 previously (116). Briefly, mid-log phase Mtb were washed in PBS repeatedly then
674 sonicated to create a single-cell suspension. Bacteria were resuspended to yield an
675 OD_{600}=0.1 in PBS. This suspension was transferred to the nebulizer of a GlassCol
676 aerosolization chamber calibrated to infect mice with ~100 bacteria per animal. On the
677 day of infection, whole lungs were collected from 5 mice per group, homogenized and
678 plated on 7H11 to determine initial inoculum. At subsequent time points, the left lung,
679 spleen and left lobe of the liver were used to determine CFU, while the right lung was
680 insuflated with 10% neutral buffered formalin for histopathology. Animal experiments
681 were reviewed and approved by the Institutional Animal Care and Use Committee at the
682 University of Texas Southwestern.
683
684 Statistical analysis
685 Statistical analysis was performed using GraphPad Prism software. For in vivo CFU
686 calculations and area of lung inflammation, the non-parametric Kruskal-Wallis test with
687 Dunn's multiple comparison was used. Analysis of survival studies was performed by
688 Kaplan-Meier test. In vitro fold CFU was calculated by dividing the average CFU of
689 quadruplicates of each Mtb strain at each time point by the average at Day 0.
690 Propagation of error (z) for each fold calculation was determined by the equation:

$$z = foldD_n \sqrt{\left(\frac{StdError\ D_n}{Avg\ D_n}\right)^2 + \left(\frac{StdError\ D_0}{Avg\ D_0}\right)^2}$$

691 where D_n represents the time point value for any given strain and D_0 represents the day
692 zero values for that given strain (117). Statistical analysis on fold CFU was performed
693 by ANOVA.
694
695 Lysozyme pull down
696 E. coli lysates containing 6x-histidine (6xHIS) tagged Mpt64 or an unrelated protein Cor
697 were incubated with cobalt affinity resin (TALON, Clontech) to bind histidine-tagged
698 proteins. After extensive washing, 1mg/mL either hen egg white or human lysozyme
699 was flowed over the immobilized beads and incubated 5 minutes. Beads were washed
700 two more times before proteins were eluted with 300mM imidazole.
701
702 Mtb genomic DNA isolation
703 Late exponential phase Mtb was collected by centrifugation and washed once in PBS.
704 Pellets were boiled 20-30 minutes to sterilize. Pellets were washed once in GTE (25mM
705 Tris, pH 8.0; 10mM EDTA; 50mM glucose) and incubated overnight in lysozyme
706 solution (10mg/mL in GTE) at 37°C. Samples were incubated in 10% SDS and
707 10mg/mL proteinase K for 40minutes at 55°C followed by incubation in NaCl and CTAB
708 (2.4M NaCl, 274mM cetrimonium bromide (Sigma)) at 60°C for 10 minutes. Genomic
709 DNA was then isolated using a phenol-chloroform extraction followed by ethanol
710 precipitation.
711

Extraction of apolar lipids and PDIM analysis

Log phage Mtb or MtbΔMpt64 were synchronized to OD_{600}=0.2 in 7H9 supplemented with 0.01% Tween 80 and grown 24 hours. Bacteria were collected by centrifugation at 1,600xg for 10 minutes, resuspended in 1mL 15% isopropanol and transferred to a glass tube containing 5mL chloroform: methanol (17:1, v/v) and incubated 24 hours at room temperature. Samples were centrifuged at 1,600xg for five minutes and the apolar lipids were collected from the bottom, organic layer and dried. Apolar lipids were resuspended in 1.5mL 100% methanol. Tween 80 was removed by addition of cobalt/thiocyanate solution and vortexed. Remaining lipids were extracted by addition of 4mL hexane. After centrifugation the organic layer was saved and the aqueous layer was re-extracted with 4mL hexane. Both hexane fractions were combined, dried and resuspended in 1mL chloroform: methanol (2:1, v/v). PDIM standard was similarly resuspended. PDIM standard, or apolar lipids extracted from Mtb or MtbΔMpt64 were infused into an AbSciex TripleTOF 5600/5600+ mass spectrometer. Samples were analyzed in the positive mode.

Acknowledgements

We would like to thank Patrick Cherry and Molly Moehlman for their contributions to this work during their summer internships. We thank BEI resources for providing reagents. This work was supported by NIH Grants R01 AI099439, R21 AI111023 and U01 AI125939 (to M.U.S.) and T32AI007520 (to C.E.S and B.L.P). M.U.S. is a Disease-Oriented Clinical Scholar at University of Texas Southwestern Medical Center.

C.E.S., N.M.A. and M.U.S. conceived and designed experiments. B.A.W. provided reagents and experimental advice. C.E.S., and S.C. performed immunofluorescence microscopy. C.E.S., B.L.P., L.H.F., and V.R.N. performed mouse aerosol infections with Mtb. B.L.P. performed mass spectrometry analysis on PDIM. C.E.S. performed the remaining research include screening experiments, molecular biology, bacterial genetics and macrophage infections. C.E.S. and M.U.S. drafted the manuscript. All authors edited and approved of the final manuscript.

References

1. WHO. 2016. Global tuberculosis report. WHO Press, World Health Organization.
2. Colditz GA, Brewer TF, Berkey CS, Wilson ME, Burdick E, Fineberg HV, Mosteller F. 1994. Efficacy of BCG vaccine in the prevention of tuberculosis. Meta-analysis of the published literature. JAMA 271:698-702.
3. Huynh KK, Joshi SA, Brown EJ. 2011. A delicate dance: host response to mycobacteria. Curr Opin Immunol 23:464-72.
4. Flannagan RS, Cosio G, Grinstein S. 2009. Antimicrobial mechanisms of phagocytes and bacterial evasion strategies. Nat Rev Microbiol 7:355-66.
5. Weiss G, Schaible UE. 2015. Macrophage defense mechanisms against intracellular bacteria. Immunol Rev 264:182-203.
6. Bradfute SB, Castillo EF, Arko-Mensah J, Chauhan S, Jiang S, Mandell M, Deretic V. 2013. Autophagy as an immune effector against tuberculosis. Current opinion in microbiology 16:355-365.

757 7. Davis AS, Vergne I, Master SS, Kyei GB, Chua J, Deretic V. 2007. Mechanism of
758 inducible nitric oxide synthase exclusion from mycobacterial phagosomes. PLoS
759 Pathog 3:e186.
760 8. Vandal OH, Pierini LM, Schnappinger D, Nathan CF, Ehrt S. 2008. A membrane
761 protein preserves intrabacterial pH in intraphagosomal Mycobacterium
762 tuberculosis. Nat Med 14:849-54.
763 9. Ehrt S, Schnappinger D. 2009. Mycobacterial survival strategies in the
764 phagosome: defence against host stresses. Cell Microbiol 11:1170-8.
765 10. Vergne I, Chua J, Singh SB, Deretic V. 2004. Cell biology of mycobacterium
766 tuberculosis phagosome. Annu Rev Cell Dev Biol 20:367-94.
767 11. Sturgill-Koszycki S, Schlesinger PH, Chakraborty P, Haddix PL, Collins HL, Fok
768 AK, Allen RD, Gluck SL, Heuser J, Russell DG. 1994. Lack of acidification in
769 Mycobacterium phagosomes produced by exclusion of the vesicular proton-
770 ATPase. Science 263:678-81.
771 12. Via LE, Deretic D, Ulmer RJ, Hibler NS, Huber LA, Deretic V. 1997. Arrest of
772 mycobacterial phagosome maturation is caused by a block in vesicle fusion
773 between stages controlled by rab5 and rab7. J Biol Chem 272:13326-31.
774 13. Pethe K, Swenson DL, Alonso S, Anderson J, Wang C, Russell DG. 2004.
775 Isolation of Mycobacterium tuberculosis mutants defective in the arrest of
776 phagosome maturation. Proc Natl Acad Sci U S A 101:13642-7.
777 14. Stewart GR, Patel J, Robertson BD, Rae A, Young DB. 2005. Mycobacterial
778 mutants with defective control of phagosomal acidification. PLoS Pathog 1:269-
779 78.

780 15. MacGurn JA, Cox JS. 2007. A genetic screen for Mycobacterium tuberculosis
781 mutants defective for phagosome maturation arrest identifies components of the
782 ESX-1 secretion system. Infect Immun 75:2668-78.
783 16. Saleh MT, Belisle JT. 2000. Secretion of an acid phosphatase (SapM) by
784 Mycobacterium tuberculosis that is similar to eukaryotic acid phosphatases. J
785 Bacteriol 182:6850-3.
786 17. Vergne I, Chua J, Lee HH, Lucas M, Belisle J, Deretic V. 2005. Mechanism of
787 phagolysosome biogenesis block by viable Mycobacterium tuberculosis. Proc
788 Natl Acad Sci U S A 102:4033-8.
789 18. Zulauf KE, Sullivan JT, Braunstein M. 2018. The SecA2 pathway of
790 Mycobacterium tuberculosis exports effectors that work in concert to arrest
791 phagosome and autophagosome maturation. PLoS Pathog 14:e1007011.
792 19. Sassetti CM, Rubin EJ. 2003. Genetic requirements for mycobacterial survival
793 during infection. Proc Natl Acad Sci U S A 100:12989-94.
794 20. Costa TR, Felisberto-Rodrigues C, Meir A, Prevost MS, Redzej A, Trokter M,
795 Waksman G. 2015. Secretion systems in Gram-negative bacteria: structural and
796 mechanistic insights. Nat Rev Microbiol 13:343-59.
797 21. Galan JE, Collmer A. 1999. Type III secretion machines: bacterial devices for
798 protein delivery into host cells. Science 284:1322-8.
799 22. Deng W, Marshall NC, Rowland JL, McCoy JM, Worrall LJ, Santos AS,
800 Strynadka NCJ, Finlay BB. 2017. Assembly, structure, function and regulation of
801 type III secretion systems. Nat Rev Microbiol 15:323-337.

802 23. Alvarez-Martinez CE, Christie PJ. 2009. Biological diversity of prokaryotic type IV
803 secretion systems. Microbiol Mol Biol Rev 73:775-808.
804 24. Ho BT, Dong TG, Mekalanos JJ. 2014. A view to a kill: the bacterial type VI
805 secretion system. Cell Host Microbe 15:9-21.
806 25. Isaac DT, Isberg R. 2014. Master manipulators: an update on Legionella
807 pneumophila Icm/Dot translocated substrates and their host targets. Future
808 Microbiol 9:343-59.
809 26. Backert S, Meyer TF. 2006. Type IV secretion systems and their effectors in
810 bacterial pathogenesis. Curr Opin Microbiol 9:207-17.
811 27. Barker JR, Chong A, Wehrly TD, Yu JJ, Rodriguez SA, Liu J, Celli J,
812 Arulanandam BP, Klose KE. 2009. The Francisella tularensis pathogenicity
813 island encodes a secretion system that is required for phagosome escape and
814 virulence. Mol Microbiol 74:1459-70.
815 28. Russell AB, Peterson SB, Mougous JD. 2014. Type VI secretion system
816 effectors: poisons with a purpose. Nat Rev Microbiol 12:137-48.
817 29. Stanley SA, Raghavan S, Hwang WW, Cox JS. 2003. Acute infection and
818 macrophage subversion by Mycobacterium tuberculosis require a specialized
819 secretion system. Proc Natl Acad Sci U S A 100:13001-6.
820 30. Groschel MI, Sayes F, Simeone R, Majlessi L, Brosch R. 2016. ESX secretion
821 systems: mycobacterial evolution to counter host immunity. Nat Rev Microbiol
822 14:677-691.
823 31. Alix E, Mukherjee S, Roy CR. 2011. Subversion of membrane transport
824 pathways by vacuolar pathogens. J Cell Biol 195:943-52.

825 32. Alto NM, Orth K. 2012. Subversion of cell signaling by pathogens. Cold Spring
826 Harb Perspect Biol 4:a006114.
827 33. Ham H, Sreelatha A, Orth K. 2011. Manipulation of host membranes by bacterial
828 effectors. Nat Rev Microbiol 9:635-46.
829 34. Boucrot E, Beuzon CR, Holden DW, Gorvel JP, Meresse S. 2003. Salmonella
830 typhimurium SifA effector protein requires its membrane-anchoring C-terminal
831 hexapeptide for its biological function. J Biol Chem 278:14196-202.
832 35. Zhao W, Moest T, Zhao Y, Guilhon AA, Buffat C, Gorvel JP, Meresse S. 2015.
833 The Salmonella effector protein SifA plays a dual role in virulence. Sci Rep
834 5:12979.
835 36. Murata T, Delprato A, Ingmundson A, Toomre DK, Lambright DG, Roy CR. 2006.
836 The Legionella pneumophila effector protein DrrA is a Rab1 guanine nucleotide-
837 exchange factor. Nat Cell Biol 8:971-7.
838 37. Niebuhr K, Giuriato S, Pedron T, Philpott DJ, Gaits F, Sable J, Sheetz MP,
839 Parsot C, Sansonetti PJ, Payrastre B. 2002. Conversion of PtdIns(4,5)P(2) into
840 PtdIns(5)P by the S.flexneri effector IpgD reorganizes host cell morphology.
841 EMBO J 21:5069-78.
842 38. Pizarro-Cerda J, Charbit A, Enninga J, Lafont F, Cossart P. 2016. Manipulation
843 of host membranes by the bacterial pathogens Listeria, Francisella, Shigella and
844 Yersinia. Semin Cell Dev Biol 60:155-167.
845 39. Weigele BA, Orchard RC, Jimenez A, Cox GW, Alto NM. 2017. A systematic
846 exploration of the interactions between bacterial effector proteins and host cell
847 membranes. Nat Commun 8:532.

848 40. Ligon LS, Hayden JD, Braunstein M. 2012. The ins and outs of Mycobacterium
849 tuberculosis protein export. Tuberculosis (Edinb) 92:121-32.
850 41. Manzanillo PS, Shiloh MU, Portnoy DA, Cox JS. 2012. Mycobacterium
851 tuberculosis activates the DNA-dependent cytosolic surveillance pathway within
852 macrophages. Cell host & microbe 11:469-480.
853 42. Stanley SA, Johndrow JE, Manzanillo P, Cox JS. 2007. The Type I IFN response
854 to infection with Mycobacterium tuberculosis requires ESX-1-mediated secretion
855 and contributes to pathogenesis. Journal of immunology (Baltimore, Md : 1950)
856 178:3143-3152.
857 43. Mehra A, Zahra A, Thompson V, Sirisaengtaksin N, Wells A, Porto M, Koster S,
858 Penberthy K, Kubota Y, Dricot A, Rogan D, Vidal M, Hill DE, Bean AJ, Philips JA.
859 2013. Mycobacterium tuberculosis type VII secreted effector EsxH targets host
860 ESCRT to impair trafficking. PLoS Pathog 9:e1003734.
861 44. Portal-Celhay C, Tufariello JM, Srivastava S, Zahra A, Klevorn T, Grace PS,
862 Mehra A, Park HS, Ernst JD, Jacobs WR, Jr., Philips JA. 2016. Mycobacterium
863 tuberculosis EsxH inhibits ESCRT-dependent CD4+ T-cell activation. Nat
864 Microbiol 2:16232.
865 45. Feltcher ME, Gunawardena HP, Zulauf KE, Malik S, Griffin JE, Sassetti CM,
866 Chen X, Braunstein M. 2015. Label-free Quantitative Proteomics Reveals a Role
867 for the Mycobacterium tuberculosis SecA2 Pathway in Exporting Solute Binding
868 Proteins and Mce Transporters to the Cell Wall. Mol Cell Proteomics 14:1501-16.
869 46. Walburger A, Koul A, Ferrari G, Nguyen L, Prescianotto-Baschong C, Huygen K,
870 Klebl B, Thompson C, Bacher G, Pieters J. 2004. Protein kinase G from

871 pathogenic mycobacteria promotes survival within macrophages. Science
872 304:1800-4.
873 47. Jimenez A, Chen D, Alto NM. 2016. How Bacteria Subvert Animal Cell Structure
874 and Function. Annu Rev Cell Dev Biol 32:373-397.
875 48. Rosenkrands I, Weldingh K, Jacobsen S, Hansen CV, Florio W, Gianetri I,
876 Andersen P. 2000. Mapping and identification of Mycobacterium tuberculosis
877 proteins by two-dimensional gel electrophoresis, microsequencing and
878 immunodetection. Electrophoresis 21:935-48.
879 49. Mattow J, Schaible UE, Schmidt F, Hagens K, Siejak F, Brestrich G, Haeselbarth
880 G, Muller EC, Jungblut PR, Kaufmann SH. 2003. Comparative proteome analysis
881 of culture supernatant proteins from virulent Mycobacterium tuberculosis H37Rv
882 and attenuated M. bovis BCG Copenhagen. Electrophoresis 24:3405-20.
883 50. Malen H, Berven FS, Fladmark KE, Wiker HG. 2007. Comprehensive analysis of
884 exported proteins from Mycobacterium tuberculosis H37Rv. Proteomics 7:1702-
885 18.
886 51. de Souza GA, Leversen NA, Malen H, Wiker HG. 2011. Bacterial proteins with
887 cleaved or uncleaved signal peptides of the general secretory pathway. J
888 Proteomics 75:502-10.
889 52. Kelkar DS, Kumar D, Kumar P, Balakrishnan L, Muthusamy B, Yadav AK,
890 Shrivastava P, Marimuthu A, Anand S, Sundaram H, Kingsbury R, Harsha HC,
891 Nair B, Prasad TS, Chauhan DS, Katoch K, Katoch VM, Kumar P, Chaerkady R,
892 Ramachandran S, Dash D, Pandey A. 2011. Proteogenomic analysis of

893 Mycobacterium tuberculosis by high resolution mass spectrometry. Mol Cell
894 Proteomics 10:M111 011627.
895 53. Conrad WH, Osman MM, Shanahan JK, Chu F, Takaki KK, Cameron J,
896 Hopkinson-Woolley D, Brosch R, Ramakrishnan L. 2017. Mycobacterial ESX-1
897 secretion system mediates host cell lysis through bacterium contact-dependent
898 gross membrane disruptions. Proc Natl Acad Sci U S A 114:1371-1376.
899 54. McCann JR, McDonough JA, Sullivan JT, Feltcher ME, Braunstein M. 2011.
900 Genome-wide identification of Mycobacterium tuberculosis exported proteins with
901 roles in intracellular growth. J Bacteriol 193:854-61.
902 55. Jungblut PR, Schaible UE, Mollenkopf HJ, Zimny-Arndt U, Raupach B, Mattow J,
903 Halada P, Lamer S, Hagens K, Kaufmann SH. 1999. Comparative proteome
904 analysis of Mycobacterium tuberculosis and Mycobacterium bovis BCG strains:
905 towards functional genomics of microbial pathogens. Mol Microbiol 33:1103-17.
906 56. Rosenkrands I, King A, Weldingh K, Moniatte M, Moertz E, Andersen P. 2000.
907 Towards the proteome of Mycobacterium tuberculosis. Electrophoresis 21:3740-
908 56.
909 57. Marjanovic O, Miyata T, Goodridge A, Kendall LV, Riley LW. 2010. Mce2 operon
910 mutant strain of Mycobacterium tuberculosis is attenuated in C57BL/6 mice.
911 Tuberculosis (Edinb) 90:50-6.
912 58. Gioffre A, Infante E, Aguilar D, Santangelo MP, Klepp L, Amadio A, Meikle V,
913 Etchechoury I, Romano MI, Cataldi A, Hernandez RP, Bigi F. 2005. Mutation in
914 mce operons attenuates Mycobacterium tuberculosis virulence. Microbes Infect
915 7:325-34.

916 59. Saini NK, Sharma M, Chandolia A, Pasricha R, Brahmachari V, Bose M. 2008.
917 Characterization of Mce4A protein of Mycobacterium tuberculosis: role in
918 invasion and survival. BMC Microbiol 8:200.
919 60. Brodin P, Poquet Y, Levillain F, Peguillet I, Larrouy-Maumus G, Gilleron M,
920 Ewann F, Christophe T, Fenistein D, Jang J, Jang MS, Park SJ, Rauzier J,
921 Carralot JP, Shrimpton R, Genovesio A, Gonzalo-Asensio JA, Puzo G, Martin C,
922 Brosch R, Stewart GR, Gicquel B, Neyrolles O. 2010. High content phenotypic
923 cell-based visual screen identifies Mycobacterium tuberculosis acyltrehalose-
924 containing glycolipids involved in phagosome remodeling. PLoS Pathog
925 6:e1001100.
926 61. Sampson SL. 2011. Mycobacterial PE/PPE proteins at the host-pathogen
927 interface. Clin Dev Immunol 2011:497203.
928 62. Bottai D, Di Luca M, Majlessi L, Frigui W, Simeone R, Sayes F, Bitter W,
929 Brennan MJ, Leclerc C, Batoni G, Campa M, Brosch R, Esin S. 2012. Disruption
930 of the ESX-5 system of Mycobacterium tuberculosis causes loss of PPE protein
931 secretion, reduction of cell wall integrity and strong attenuation. Mol Microbiol
932 83:1195-209.
933 63. Shah S, Briken V. 2016. Modular Organization of the ESX-5 Secretion System in
934 Mycobacterium tuberculosis. Front Cell Infect Microbiol 6:49.
935 64. Sassetti CM, Boyd DH, Rubin EJ. 2003. Genes required for mycobacterial growth
936 defined by high density mutagenesis. Mol Microbiol 48:77-84.

937 65. Rengarajan J, Bloom BR, Rubin EJ. 2005. Genome-wide requirements for
938 Mycobacterium tuberculosis adaptation and survival in macrophages. Proc Natl
939 Acad Sci U S A 102:8327-32.
940 66. Rosas-Magallanes V, Stadthagen-Gomez G, Rauzier J, Barreiro LB, Tailleux L,
941 Boudou F, Griffin R, Nigou J, Jackson M, Gicquel B, Neyrolles O. 2007.
942 Signature-tagged transposon mutagenesis identifies novel Mycobacterium
943 tuberculosis genes involved in the parasitism of human macrophages. Infect
944 Immun 75:504-7.
945 67. Isakoff SJ, Cardozo T, Andreev J, Li Z, Ferguson KM, Abagyan R, Lemmon MA,
946 Aronheim A, Skolnik EY. 1998. Identification and analysis of PH domain-
947 containing targets of phosphatidylinositol 3-kinase using a novel in vivo assay in
948 yeast. EMBO J 17:5374-87.
949 68. Aronheim A, Zandi E, Hennemann H, Elledge SJ, Karin M. 1997. Isolation of an
950 AP-1 repressor by a novel method for detecting protein-protein interactions. Mol
951 Cell Biol 17:3094-102.
952 69. Chiu VK, Bivona T, Hach A, Sajous JB, Silletti J, Wiener H, Johnson RL, 2nd,
953 Cox AD, Philips MR. 2002. Ras signalling on the endoplasmic reticulum and the
954 Golgi. Nat Cell Biol 4:343-50.
955 70. Yu JW, Mendrola JM, Audhya A, Singh S, Keleti D, DeWald DB, Murray D, Emr
956 SD, Lemmon MA. 2004. Genome-wide analysis of membrane targeting by S.
957 cerevisiae pleckstrin homology domains. Mol Cell 13:677-88.
958 71. Personnic N, Barlocher K, Finsel I, Hilbi H. 2016. Subversion of Retrograde
959 Trafficking by Translocated Pathogen Effectors. Trends Microbiol 24:450-62.

960 72. Sullivan JT, Young EF, McCann JR, Braunstein M. 2012. The Mycobacterium
961 tuberculosis SecA2 system subverts phagosome maturation to promote growth in
962 macrophages. Infect Immun 80:996-1006.
963 73. Bach H, Papavinasasundaram KG, Wong D, Hmama Z, Av-Gay Y. 2008.
964 Mycobacterium tuberculosis virulence is mediated by PtpA dephosphorylation of
965 human vacuolar protein sorting 33B. Cell Host Microbe 3:316-22.
966 74. Rivera VM, Wang X, Wardwell S, Courage NL, Volchuk A, Keenan T, Holt DA,
967 Gilman M, Orci L, Cerasoli F, Jr., Rothman JE, Clackson T. 2000. Regulation of
968 protein secretion through controlled aggregation in the endoplasmic reticulum.
969 Science 287:826-30.
970 75. Selyunin AS, Sutton SE, Weigele BA, Reddick LE, Orchard RC, Bresson SM,
971 Tomchick DR, Alto NM. 2011. The assembly of a GTPase-kinase signalling
972 complex by a bacterial catalytic scaffold. Nature 469:107-11.
973 76. Selyunin AS, Reddick LE, Weigele BA, Alto NM. 2014. Selective protection of an
974 ARF1-GTP signaling axis by a bacterial scaffold induces bidirectional trafficking
975 arrest. Cell Rep 6:878-91.
976 77. Shenoy VP, Mukhopadhyay C. 2014. Rapid Immunochromatographic Test for the
977 Identification and Discrimination of Mycobacterium tuberculosis Complex Isolates
978 from Non-tuberculous Mycobacteria. J Clin Diagn Res 8:DC13-5.
979 78. Arora J, Kumar G, Verma AK, Bhalla M, Sarin R, Myneedu VP. 2015. Utility of
980 MPT64 Antigen Detection for Rapid Confirmation of Mycobacterium tuberculosis
981 Complex. J Glob Infect Dis 7:66-9.

982 79. Behr MA, Wilson MA, Gill WP, Salamon H, Schoolnik GK, Rane S, Small PM.
983 1999. Comparative genomics of BCG vaccines by whole-genome DNA
984 microarray. Science 284:1520-3.
985 80. Kozak RA, Alexander DC, Liao R, Sherman DR, Behr MA. 2011. Region of
986 difference 2 contributes to virulence of Mycobacterium tuberculosis. Infect Immun
987 79:59-66.
988 81. Sonnenberg MG, Belisle JT. 1997. Definition of Mycobacterium tuberculosis
989 culture filtrate proteins by two-dimensional polyacrylamide gel electrophoresis, N-
990 terminal amino acid sequencing, and electrospray mass spectrometry. Infect
991 Immun 65:4515-24.
992 82. Wang Z, Potter BM, Gray AM, Sacksteder KA, Geisbrecht BV, Laity JH. 2007.
993 The solution structure of antigen MPT64 from Mycobacterium tuberculosis
994 defines a new family of beta-grasp proteins. J Mol Biol 366:375-81.
995 83. Hastie JL, Williams KB, Bohr LL, Houtman JC, Gakhar L, Ellermeier CD. 2016.
996 The Anti-sigma Factor RsiV Is a Bacterial Receptor for Lysozyme: Co-crystal
997 Structure Determination and Demonstration That Binding of Lysozyme to RsiV Is
998 Required for sigmaV Activation. PLoS Genet 12:e1006287.
999 84. Kelley LA, Mezulis S, Yates CM, Wass MN, Sternberg MJ. 2015. The Phyre2
1000 web portal for protein modeling, prediction and analysis. Nat Protoc 10:845-58.
1001 85. Breker M, Gymrek M, Schuldiner M. 2013. A novel single-cell screening platform
1002 reveals proteome plasticity during yeast stress responses. J Cell Biol 200:839-
1003 50.

1004 86. Huh WK, Falvo JV, Gerke LC, Carroll AS, Howson RW, Weissman JS, O'Shea
1005 EK. 2003. Global analysis of protein localization in budding yeast. Nature
1006 425:686-91.
1007 87. Champion PA, Stanley SA, Champion MM, Brown EJ, Cox JS. 2006. C-terminal
1008 signal sequence promotes virulence factor secretion in Mycobacterium
1009 tuberculosis. Science 313:1632-6.
1010 88. Hsu T, Hingley-Wilson SM, Chen B, Chen M, Dai AZ, Morin PM, Marks CB,
1011 Padiyar J, Goulding C, Gingery M, Eisenberg D, Russell RG, Derrick SC, Collins
1012 FM, Morris SL, King CH, Jacobs WR, Jr. 2003. The primary mechanism of
1013 attenuation of bacillus Calmette-Guerin is a loss of secreted lytic function
1014 required for invasion of lung interstitial tissue. Proc Natl Acad Sci U S A
1015 100:12420-5.
1016 89. van der Wel N, Hava D, Houben D, Fluitsma D, van Zon M, Pierson J, Brenner
1017 M, Peters PJ. 2007. M. tuberculosis and M. leprae translocate from the
1018 phagolysosome to the cytosol in myeloid cells. Cell 129:1287-98.
1019 90. Bardarov S, Kriakov J, Carriere C, Yu S, Vaamonde C, McAdam RA, Bloom BR,
1020 Hatfull GF, Jacobs WR, Jr. 1997. Conditionally replicating mycobacteriophages:
1021 a system for transposon delivery to Mycobacterium tuberculosis. Proc Natl Acad
1022 Sci U S A 94:10961-6.
1023 91. Glickman MS, Cox JS, Jacobs WR, Jr. 2000. A novel mycolic acid cyclopropane
1024 synthetase is required for cording, persistence, and virulence of Mycobacterium
1025 tuberculosis. Mol Cell 5:717-27.

1026 92. Glickman MS, Cahill SM, Jacobs WR, Jr. 2001. The Mycobacterium tuberculosis
1027 cmaA2 gene encodes a mycolic acid trans-cyclopropane synthetase. J Biol
1028 Chem 276:2228-33.
1029 93. Chan K, Knaak T, Satkamp L, Humbert O, Falkow S, Ramakrishnan L. 2002.
1030 Complex pattern of Mycobacterium marinum gene expression during long-term
1031 granulomatous infection. Proc Natl Acad Sci U S A 99:3920-5.
1032 94. Brennan MJ. 2017. The Enigmatic PE/PPE Multigene Family of Mycobacteria
1033 and Tuberculosis Vaccination. Infect Immun 85.
1034 95. Perkowski EF, Zulauf KE, Weerakoon D, Hayden JD, Ioerger TR, Oreper D,
1035 Gomez SM, Sacchettini JC, Braunstein M. 2017. The EXIT Strategy: an
1036 Approach for Identifying Bacterial Proteins Exported during Host Infection. MBio
1037 8.
1038 96. Sun J, Singh V, Lau A, Stokes RW, Obregón-Henao A, Orme IM, Wong D, Av-
1039 Gay Y, Hmama Z. 2013. Mycobacterium tuberculosis nucleoside diphosphate
1040 kinase inactivates small GTPases leading to evasion of innate immunity. PLoS
1041 pathogens 9:e1003499.
1042 97. Khan S, Islam A, Hassan MI, Ahmad F. 2016. Purification and structural
1043 characterization of Mce4A from Mycobacterium tuberculosis. Int J Biol Macromol
1044 93:235-241.
1045 98. Daleke MH, Cascioferro A, de Punder K, Ummels R, Abdallah AM, van der Wel
1046 N, Peters PJ, Luirink J, Manganelli R, Bitter W. 2011. Conserved Pro-Glu (PE)
1047 and Pro-Pro-Glu (PPE) protein domains target LipY lipases of pathogenic

1048 mycobacteria to the cell surface via the ESX-5 pathway. J Biol Chem 286:19024-
1049 34.
1050 99. de Jonge MI, Pehau-Arnaudet G, Fretz MM, Romain F, Bottai D, Brodin P,
1051 Honore N, Marchal G, Jiskoot W, England P, Cole ST, Brosch R. 2007. ESAT-6
1052 from Mycobacterium tuberculosis Dissociates from Its Putative Chaperone CFP-
1053 10 under Acidic Conditions and Exhibits Membrane-Lysing Activity. Journal of
1054 Bacteriology 189:6028-6034.
1055 100. Smith J, Manoranjan J, Pan M, Bohsali A, Xu J, Liu J, McDonald KL, Szyk A,
1056 LaRonde-LeBlanc N, Gao LY. 2008. Evidence for pore formation in host cell
1057 membranes by ESX-1-secreted ESAT-6 and its role in Mycobacterium marinum
1058 escape from the vacuole. Infect Immun 76:5478-87.
1059 101. Danilchanka O, Sun J, Pavlenok M, Maueroder C, Speer A, Siroy A, Marrero J,
1060 Trujillo C, Mayhew DL, Doornbos KS, Munoz LE, Herrmann M, Ehrt S, Berens C,
1061 Niederweis M. 2014. An outer membrane channel protein of Mycobacterium
1062 tuberculosis with exotoxin activity. Proc Natl Acad Sci U S A 111:6750-5.
1063 102. Sun J, Siroy A, Lokareddy RK, Speer A, Doornbos KS, Cingolani G, Niederweis
1064 M. 2015. The tuberculosis necrotizing toxin kills macrophages by hydrolyzing
1065 NAD. Nat Struct Mol Biol 22:672-8.
1066 103. De Matteis MA, Wilson C, D'Angelo G. 2013. Phosphatidylinositol-4-phosphate:
1067 the Golgi and beyond. Bioessays 35:612-22.
1068 104. Matsuoka K, Orci L, Amherdt M, Bednarek SY, Hamamoto S, Schekman R,
1069 Yeung T. 1998. COPII-coated vesicle formation reconstituted with purified coat
1070 proteins and chemically defined liposomes. Cell 93:263-75.

1071 105. Blumental-Perry A, Haney CJ, Weixel KM, Watkins SC, Weisz OA, Aridor M.
1072 2006. Phosphatidylinositol 4-phosphate formation at ER exit sites regulates ER
1073 export. Dev Cell 11:671-82.
1074 106. Sarkes D, Rameh LE. 2010. A novel HPLC-based approach makes possible the
1075 spatial characterization of cellular PtdIns5P and other phosphoinositides.
1076 Biochem J 428:375-84.
1077 107. Choi S, Thapa N, Tan X, Hedman AC, Anderson RA. 2015. PIP kinases define
1078 PI4,5P(2)signaling specificity by association with effectors. Biochim Biophys Acta
1079 1851:711-23.
1080 108. Manna P, Jain SK. 2015. Phosphatidylinositol-3,4,5-triphosphate and cellular
1081 signaling: implications for obesity and diabetes. Cell Physiol Biochem 35:1253-
1082 75.
1083 109. O'Connor TJ, Adepoju Y, Boyd D, Isberg RR. 2011. Minimization of the
1084 Legionella pneumophila genome reveals chromosomal regions involved in host
1085 range expansion. Proc Natl Acad Sci U S A 108:14733-40.
1086 110. Ensminger AW. 2016. Legionella pneumophila, armed to the hilt: justifying the
1087 largest arsenal of effectors in the bacterial world. Curr Opin Microbiol 29:74-80.
1088 111. Behar SM, Martin CJ, Nunes-Alves C, Divangahi M, Remold HG. 2011. Lipids,
1089 apoptosis, and cross-presentation: links in the chain of host defense against
1090 Mycobacterium tuberculosis. Microbes Infect 13:749-56.
1091 112. Roche PW, Triccas JA, Avery DT, Fifis T, Billman-Jacobe H, Britton WJ. 1994.
1092 Differential T cell responses to mycobacteria-secreted proteins distinguish

1093 vaccination with bacille Calmette-Guerin from infection with Mycobacterium
1094 tuberculosis. J Infect Dis 170:1326-30.
1095 113. Roche PW, Feng CG, Britton WJ. 1996. Human T-cell epitopes on the
1096 Mycobacterium tuberculosis secreted protein MPT64. Scand J Immunol 43:662-
1097 70.
1098 114. Mustafa T, Wiker HG, Morkve O, Sviland L. 2007. Reduced apoptosis and
1099 increased inflammatory cytokines in granulomas caused by tuberculous
1100 compared to non-tuberculous mycobacteria: role of MPT64 antigen in apoptosis
1101 and immune response. Clin Exp Immunol 150:105-13.
1102 115. Mustafa T, Wiker HG, Morkve O, Sviland L. 2008. Differential expression of
1103 mycobacterial antigen MPT64, apoptosis and inflammatory markers in
1104 multinucleated giant cells and epithelioid cells in granulomas caused by
1105 Mycobacterium tuberculosis. Virchows Arch 452:449-56.
1106 116. Collins AC, Cai H, Li T, Franco LH, Li XD, Nair VR, Scharn CR, Stamm CE,
1107 Levine B, Chen ZJ, Shiloh MU. 2015. Cyclic GMP-AMP Synthase Is an Innate
1108 Immune DNA Sensor for Mycobacterium tuberculosis. Cell Host Microbe 17:820-
1109 8.
1110 117. Ku HH. 1966. Notes on the Use of Propagation of Error Formulas. Journal Of
1111 Research of the National Bureau of Standards - C Engineering and
1112 Instrumentation 70C:263-273.
1113

Figure legends

Figure 1. *M. tuberculosis* exported proteins interact with yeast membranes. (**A**) Ras rescue assay schematic. (**B**) *S. cerevisiae* (cdc25^{ts}) transformed with Mtb protein fusions to Ras^{mut}, duplicate plated and incubated 48-72 h at the permissive (25°C) and restrictive (37°C) temperatures. Shown are representative images of 20 yeast strains. (**C**) Summary results of Ras rescue screen. (**D**) Western blot of lysates from yeast transformed with the indicated fusion proteins and probed with anti-Ras or anti-G6PDH antibodies. Ras^{mut} fusion proteins are marked by white or black asterisks. PLC (phospholipase C) and DYN (dynamin) are fusions to Ras^{mut} known to be membrane associated (PLC) or cytoplasmic (DYN). (**E**) Representative fluorescence microscopy of *S. cerevisiae* (INVSc1) transformed with GFP-MEP fusion proteins. Scale bars are 3μm.

Figure 2. Host subcellular localization of membrane-binding MEP. (**A**) Representative fluorescent images of HeLa cells transfected with the indicated GFP-MEP fusion proteins (green) and stained with antibodies (red) to calreticulin (ER), GM-130 (Golgi), Tom20 (Mitochondria) or PMP70 (Peroxisomes). Scale bars are 5μm. (**B**) Comparison of the organelle localization of MEP expressed in yeast and HeLa cells.

Figure 3. *M. tuberculosis* exported proteins alter hGH secretion (**A**) Inducible secretion assay schematic. (**B**) Supernatant hGH ELISA from HeLa cells transfected overnight with hGH-CAD and either GFP or GFP-MEP fusion proteins prior to addition of drug to allow for hGH secretion. hGH secretion by GFP-MEP transfected cells was normalized to hGH secretion of cells transfected with GFP alone. (**C**) Summary of results from

1137 inducible secretion screen. (**D**) Venn diagram of MEP that are membrane-localized,
1138 alter host secretion, or both. (**E**) Table summarizing the membrane localization and
1139 degree of hGH secretion in cells transfected with the five overlapping proteins from **D**.
1140

1141 Figure 4. hGH secretion inhibition is dependent on membrane localization of Mpt64. (**A**)
1142 Solution structure of Mpt64. PDB 2hhi. (**B**) Schematic of Mpt64 truncations, colored to
1143 match solution structure in **A**. SP, signal peptide. (**C**) Full length Mpt64 or protein
1144 truncations expressed in the Ras rescue assay. (**D**) Western blot of lysates from $cdc25^{ts}$
1145 yeast expressing Ras^{mut} fusion proteins to Mpt64 or Mpt64 truncations. Blots were
1146 probed for anti-Ras or anti-G6PDH antibodies. Control protein bands are marked by a
1147 white asterisk and Mpt64 truncations are marked by a black asterisk. (**E**) PIP
1148 membrane strips incubated with recombinant Mpt64_24-228 or Mpt64_24-143. Binding
1149 of Mpt64 to lipids was detected by incubation with α-Mpt64 or pre-immune serum.
1150 Numbers indicate specific lipids as follows: 1, lysophosphatidic acid; 2,
1151 lysophosphatidylcholine; 3, phosphatidylinositol; 4, phosphatidylinositol-3-phopshate
1152 (PI3P); 5, PI4P; 6, PI5P; 7, phosphatidylethanolamine; 8, phosphatidylcholine; 9,
1153 sphingosine 1-phosophate; 10, phosphatidylinositol-3,4-bisphosphate [$PI(3,4)P_2$]; 11,
1154 $PI(3,5)P_2$; 12, $PI(4,5)P_2$; 13, phosphatidylinositol-3,4,5-trisphosphate [$PI(3,4,5)P_3$]; 14,
1155 phosphatidic acid; 15, phosphatidylserine; 16, blank. (**F**) ELISA results of hGH in
1156 supernatants of cells co-expressing full length Mpt64, Mpt64 truncations or controls.
1157

1158 Figure 5. Mpt64 localizes to the endoplasmic reticulum during heterologous expression
1159 in yeast and HeLa cells. (**A**) Immunofluorescence (top panels) and bright field overlay

1160 (bottom panels) images of *S. cerevisiae* transformed with GFP fusion proteins to Mpt64
1161 truncations. Scale bars are 3 μm. (**B**) HeLa cells transfected overnight with GFP fusion
1162 proteins (green) and stained for ER localization with anti-calreticulin antibody (red).
1163 Nuclei are stained with DAPI (blue). Scale bars are 10 μm.
1164
1165 Figure 6. Mpt64 ER localization is ESX1-dependant during *M. tuberculosis* infection of
1166 macrophages. (**A**) RAW267.4 murine macrophages were infected with mCherry-
1167 expressing (red) WT (upper panels) or MtbΔeccD1 (lower panels) for 4 hours at an MOI
1168 20:1. Cells were fixed and stained for Mpt64 (green) and nuclei (blue). Scale bars are
1169 5μm. (**B**) Schematic detailing in-frame deletion of *mpt64* by insertion of a hygromycin
1170 resistance gene. (**C**) Western blot detecting expression of Mpt64, Ag85 and GroEL2 in
1171 either the lysate of the cell pellet (P) or culture supernatant (S) of four Mtb strains. (**D**)
1172 RAW267.4 macrophages were infected with the indicated strains of mCherry-
1173 expressing (cyan) Mtb for 4 hours at an MOI 20:1. Cells were fixed and stained for
1174 Mpt64 (red), calreticulin (green) and nuclei (blue). Images in (**E**) and (**F**) correspond to
1175 box 1 and box 2, respectively. Scale bars are 10μm. (**E**) Enlarged image from box 1 in
1176 (**D**) of an Mtb-infected macrophage stained for Mpt64, calreticulin and DAPI. Insets
1177 show an area of Mpt64-calreticulin co-localization. Scale bars are 5μm. (**F**) Enlarged
1178 image from box 2 in (**D**) of macrophages infected with MtbΔMpt64::Mpt64-NS and
1179 stained for Mpt64, calreticulin and DAPI. Insets show Mpt64 localization in relation to
1180 bacteria. Scale bars are 5 μm.
1181

1182 Figure 7. Mpt64 contributes to early Mtb growth after aerosol infection of mice (**A**)
1183 Bacterial burden in lungs of mice 21 and 42 days after aerosol infection with indicated
1184 strains of Mtb. Results are a combination of three independent experiments, n=25 mice
1185 total per group. Horizontal bar indicates the geometric mean. p values are determined
1186 by nonparametric Kruskal-Wallis analysis. (**B**) Representative images of H&E stained
1187 lungs at 42 days post-infection with the indicated strains of Mtb. Scale bars, 2mm. (**C**)
1188 Ten mice per group were monitored for survival. There were no significant differences in
1189 survival rates between groups by Kaplan–Meier analysis. (**D**) Quantitation of lung
1190 inflammation of mice infected with indicated Mtb strains. Measurement was determined
1191 using ImageJ software (NIH). Bars are colored as in (**A**). Results are the mean ±SEM
1192 for three animals per group. *p<0.02 by Kruskal-Wallis test.
1193
1194 Figure 8. Localization and activity of Mpt64 in human macrophages (**A**) Primary human
1195 monocyte-derived macrophages were infected with mCherry-expressing (red) Mtb or
1196 MtbΔeccD1 for 4 hours at an MOI 10:1. Cells were fixed and stained for Mpt64 (green).
1197 Scale bars are 5μm. (**B**) Primary human monocyte-derived macrophages were infected
1198 with the indicated strains of mCherry-expressing Mtb for 4 hours at an MOI 10:1. Cells
1199 were fixed and stained for Mpt64 (red) and calreticulin (green). Nuclei are stained blue.
1200 Scale bars are 5 μm and scale bars of inset images are 2.5 μm. (**C**) CFU recovered
1201 from primary human macrophages from two separate donors infected with Mtb,
1202 MtbΔMpt64, or MtbΔMpt64::Mpt64 at indicated time points. CFU was normalized to the
1203 bacterial burden at day 0 and is represented as the mean with standard error. Data are
1204 representative of 6 independent experiments.

1205

1206 Supplemental Figure 1. Recombinant Mpt64 does not interact with lysozyme. (**A**)
1207 Sequence and secondary structure alignment of Mpt64 and *B. subtilis* RsiV (template)
1208 performed by Phyre[2] software (http://www.sbg.bio.ic.ac.uk/phyre2/). The Mpt64
1209 DUF3298 is indicated by a red line above the Mpt64 amino acid numbering. (**B**) Mpt64
1210 (M) or an unrelated protein Cor (C) were immobilized on cobalt beads and hen egg
1211 white (HEW) or human lysozyme (HuLYZ) was incubated with these or beads alone (B)
1212 for five minutes. After washes, proteins were eluted with 300mM imidazole.

1213

1214 Supplemental Figure 2. Construction and phenotypic analysis of MtbΔMpt64. (**A**)
1215 Western blot detecting expression of Mpt64, Ag85 and GroEL2 in either the lysate of the
1216 cell pellet (P) or culture supernatant (S) of wild type Mtb or MtbΔeccD1. (**B**) Detection of
1217 hygromycin resistance cassette insertion in place of *mpt64*. Genomic DNA from wild
1218 type Mtb or MtbΔMpt64 was amplified by polymerase chain reaction and products were
1219 analyzed by agarose gel electrophoresis. (**C**) Growth of Mtb, MtbΔMpt64,
1220 MtbΔMpt64::Mpt64 and MtbΔMpt64::Mpt64-NS in 7H9 measured by optical density at
1221 600nm. (**D**) PDIM standard or apolar lipid extracts from Mtb or MtbΔMpt64 were
1222 analyzed on an AbSciex TripleTOF 5600/5600+ mass spectrometer.

1223

1224 Supplemental Figure 3. Secreted Mpt64 co-localizes with calreticulin in murine
1225 macrophages. (A) RAW267.4 murine macrophages were infected with the indicated
1226 strains of mCherry expressing Mtb (cyan) for four hours and subsequently stained for
1227 Mpt64 (red) and calreticulin (green). Nuclei are stained in blue. Scale bars are 10μm.

1228

1229 Supplemental Figure 4. Secreted Mpt64 co-localizes with calreticulin in human
1230 macrophages. (A) Primary human macrophages were infected with the indicated strains
1231 of mCherry expressing Mtb (cyan) or left uninfected for four hours prior to fixation and
1232 staining for Mpt64 (red) and calreticulin (green). Scale bars are 5μm.

Figure 1

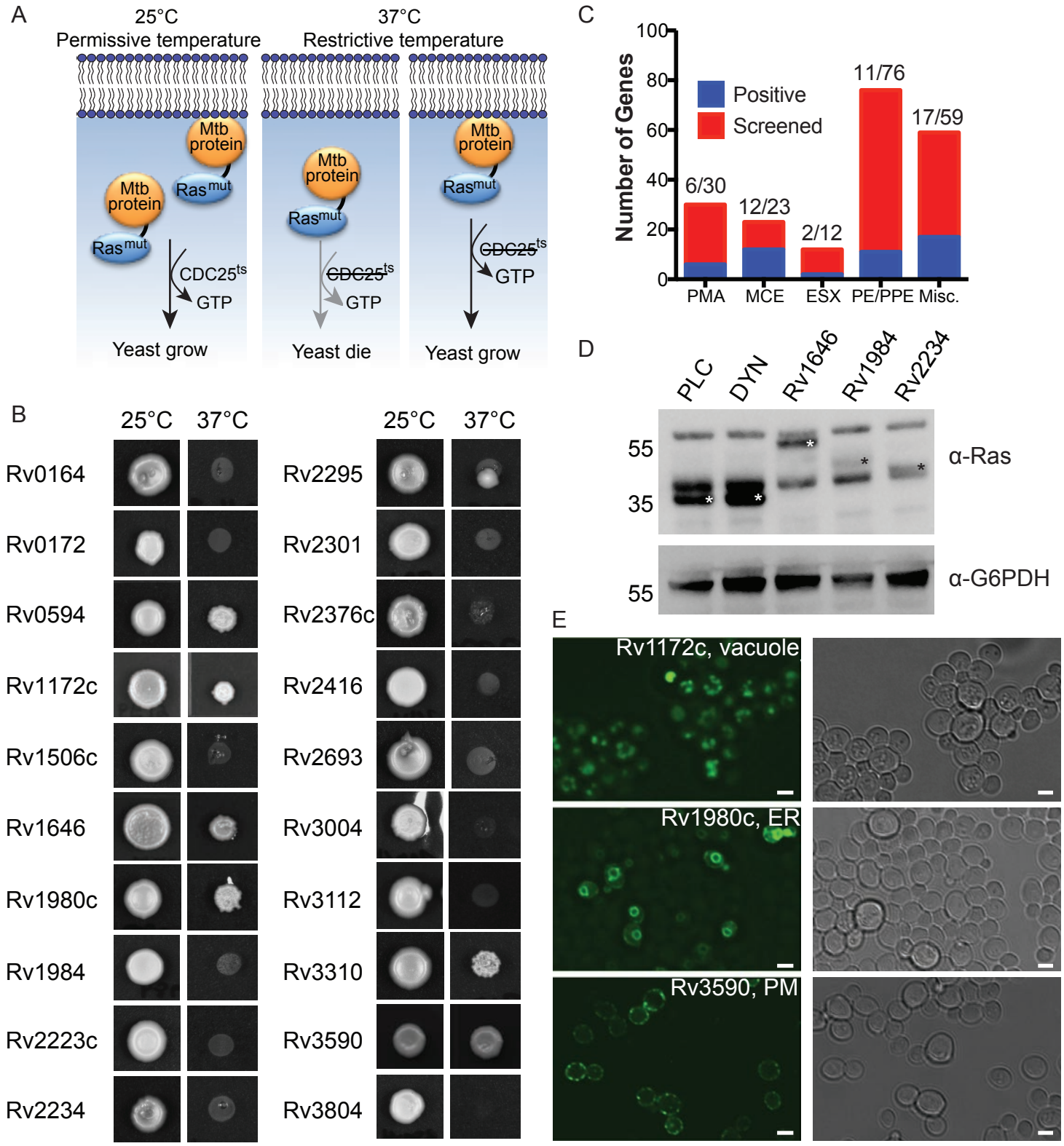

Figure 1. M. tuberculosis exported proteins interact with yeast membranes. (A) Ras rescue assay schematic. (B) S. cerevisiae (cdc25ts) transformed with Mtb protein fusions to Rasmut, duplicate plated and incubated 48-72 h at the permissive (25°C) and restrictive (37°C) temperatures. Shown are representative images of 20 yeast strains. (C) Summary results of Ras rescue screen. (D) Western blot of lysates from yeast transformed with the indicated fusion proteins and probed with anti-Ras or anti-G6PDH antibodies. Rasmut fusion proteins are marked by white or black asterisks. PLC (phospholipase C) and DYN (dynamin) are fusions to Rasmut known to be membrane associated (PLC) or cytoplasmic (DYN). (E) Representative fluorescence microscopy of S. cerevisiae (INVSc1) transformed with GFP-MEP fusion proteins. Scale bars are 3μm.

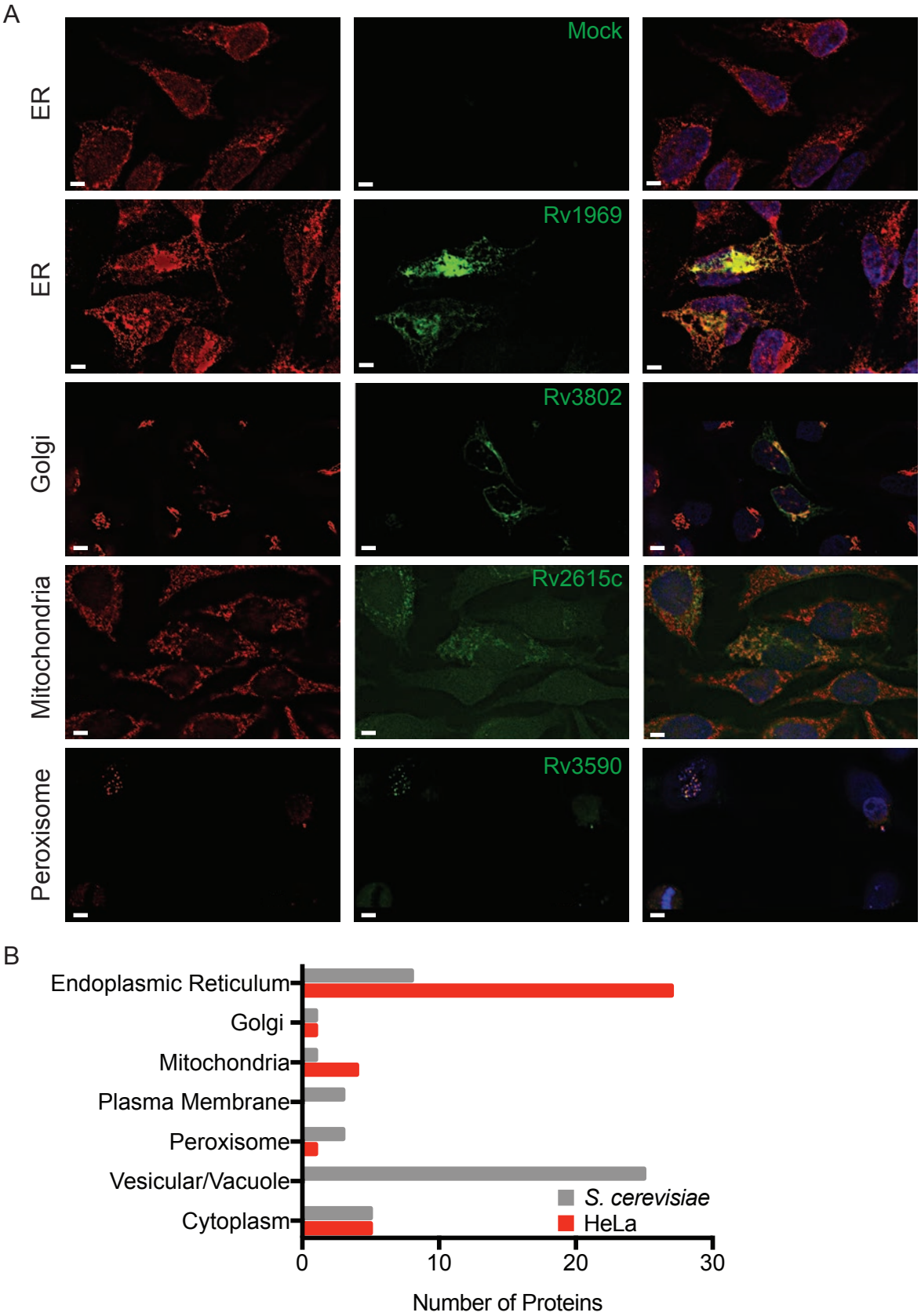

Figure 2. Host subcellular localization of membrane-binding MEP. (A) Representative fluorescent images of HeLa cells transfected with the indicated GFP-MEP fusion proteins (green) and stained with antibodies (red) to calreticulin (ER), GM-130 (Golgi), Tom20 (Mitochondria) or PMP70 (Peroxisomes). Scale bars are 5μm. (B) Comparison of the organelle localization of MEP expressed in yeast and HeLa cells.

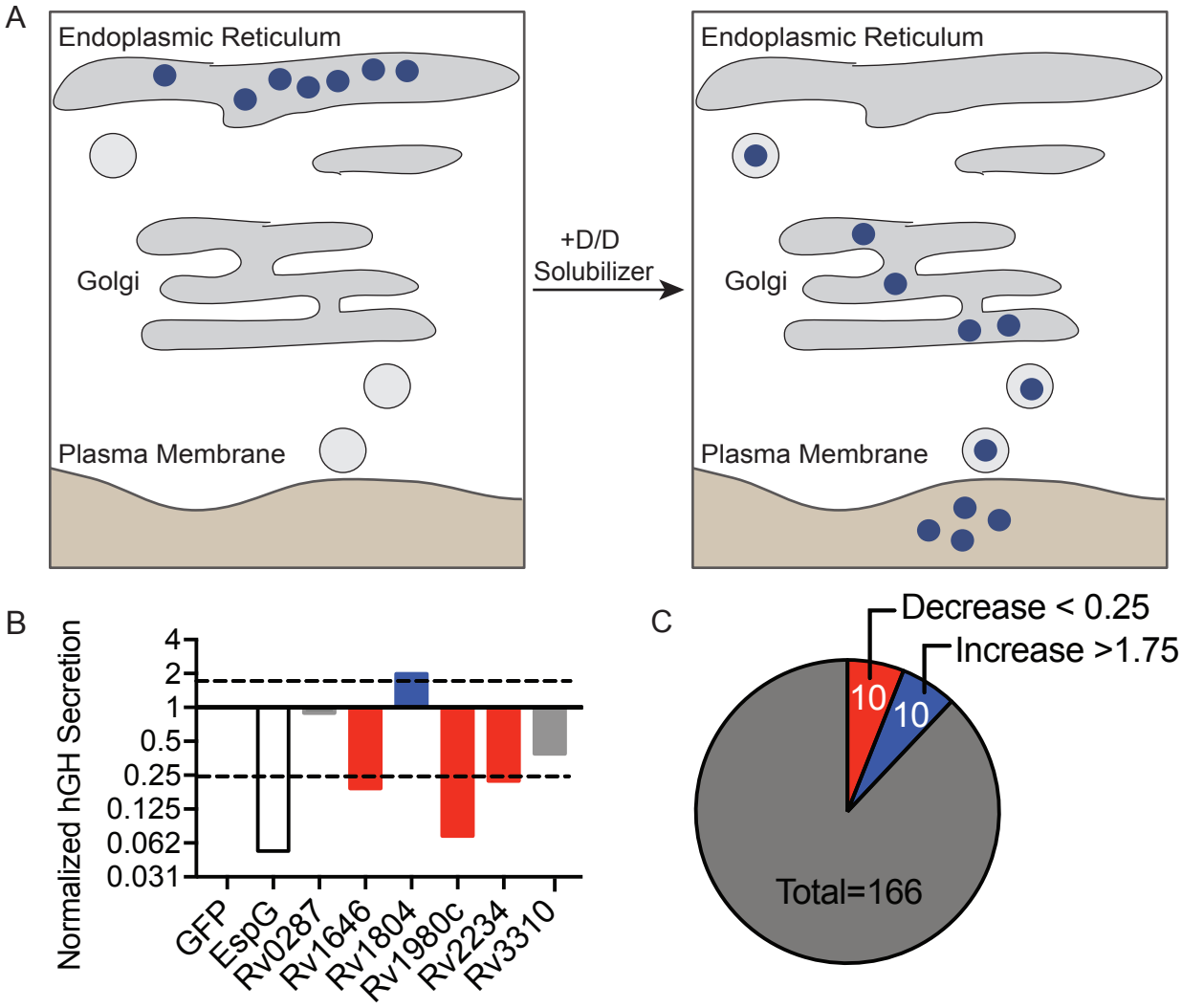

D

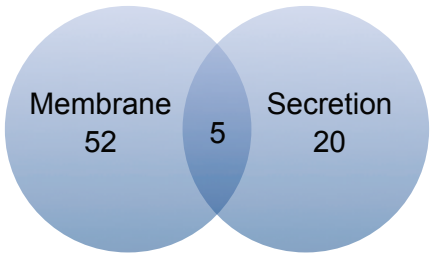

E

Gene	Localization	hGH Secretion
Rv0549	ER	0.194
Rv1646	Mitochondria	0.191
Rv1810	ER	0.203
Rv1980c	ER	0.072
Rv2295	ER	0.213

Figure 3. M. tuberculosis exported proteins alter hGH secretion (A) Inducible secretion assay schematic. (B) Supernatant hGH ELISA from HeLa cells transfected overnight with hGH-CAD and either GFP or GFP-MEP fusion proteins prior to addition of drug to allow for hGH secretion. hGH secretion by GFP-MEP transfected cells was normalized to hGH secretion of cells transfected with GFP alone. (C) Summary of results from inducible secretion screen. (D) Venn diagram of MEP that are membrane-localized, alter host secretion, or both. (E) Table summarizing the membrane localization and degree of hGH secretion in cells transfected with the five overlapping proteins from D.

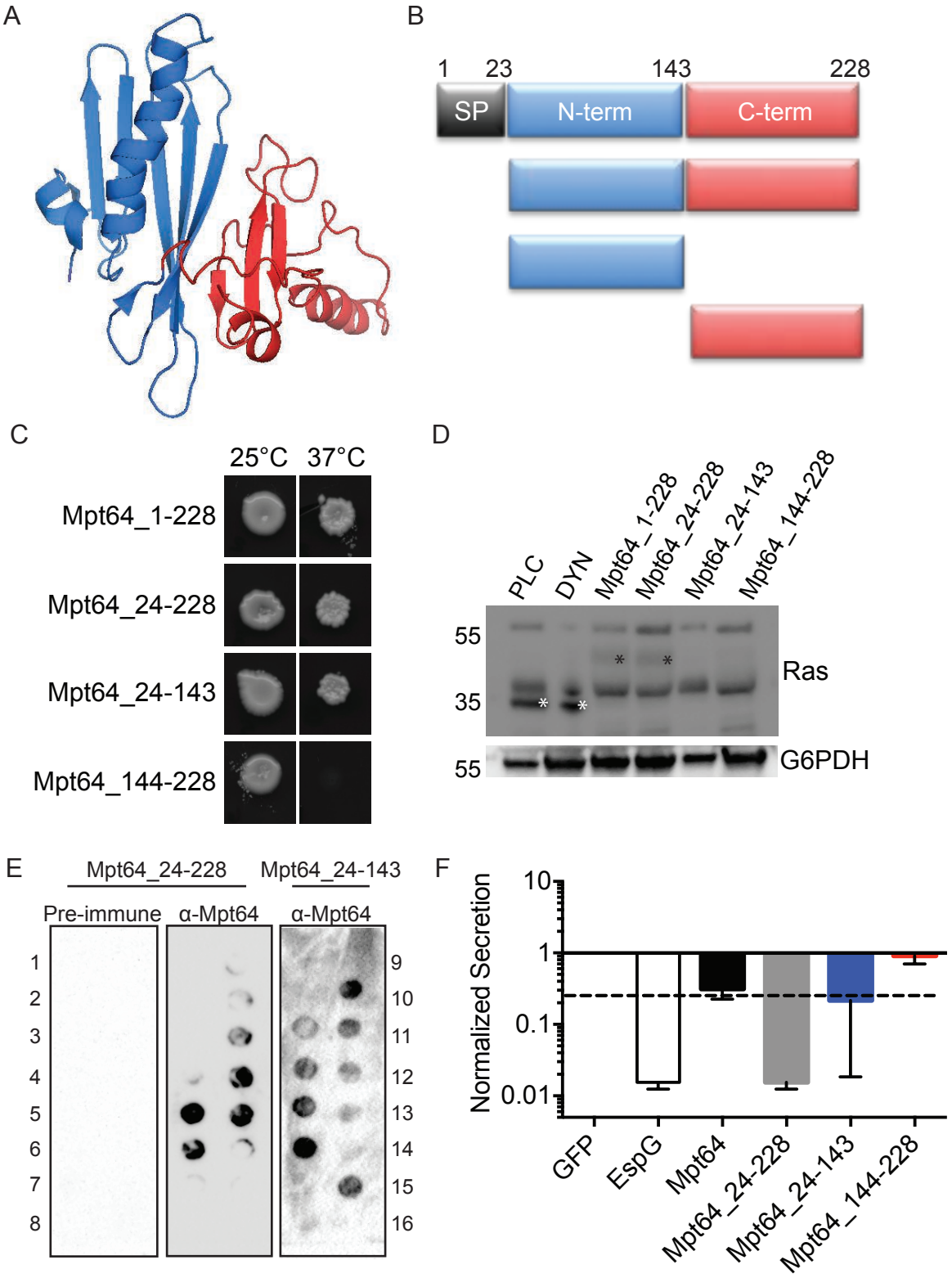

Figure 4. hGH secretion inhibition is dependent on membrane localization of Mpt64. (A) Solution structure of Mpt64. PDB 2hhi. (B) Schematic of Mpt64 truncations, colored to match solution structure in A. SP, signal peptide. (C) Full length Mpt64 or protein truncations expressed in the Ras rescue assay. (D) Western blot of lysates from cdc25ts yeast expressing Rasmut fusion proteins to Mpt64 or Mpt64 truncations. Blots were probed for anti-Ras or anti-G6PDH antibodies. Control protein bands are marked by a white asterisk and Mpt64 truncations are marked by a black asterisk. (E) PIP membrane strips incubated with recombinant Mpt64_24-228 or Mpt64_24-143. Binding of Mpt64 to lipids was detected by incubation with α-Mpt64 or pre-immune serum. Numbers indicate specific lipids as follows:
1, lysophosphatidic acid; 2, lysophosphatidylcholine; 3, phosphatidylinositol; 4, phosphatidylinositol-3-phopshate (PI3P); 5, PI4P; 6, PI5P; 7, phosphatidylethanolamine; 8, phosphatidylcholine; 9, sphingosine 1-phosophate;
10, phosphatidylinositol-3,4-bisphosphate [PI(3,4)P2]; 11, PI(3,5)P2; 12, PI(4,5)P2; 13, phosphatidylinositol-3,4,5-trisphosphate [PI(3,4,5)P3]; 14, phosphatidic acid; 15, phosphatidylserine; 16, blank. (F) ELISA results of hGH in supernatants of cells co-expressing full length Mpt64, Mpt64 truncations or controls.

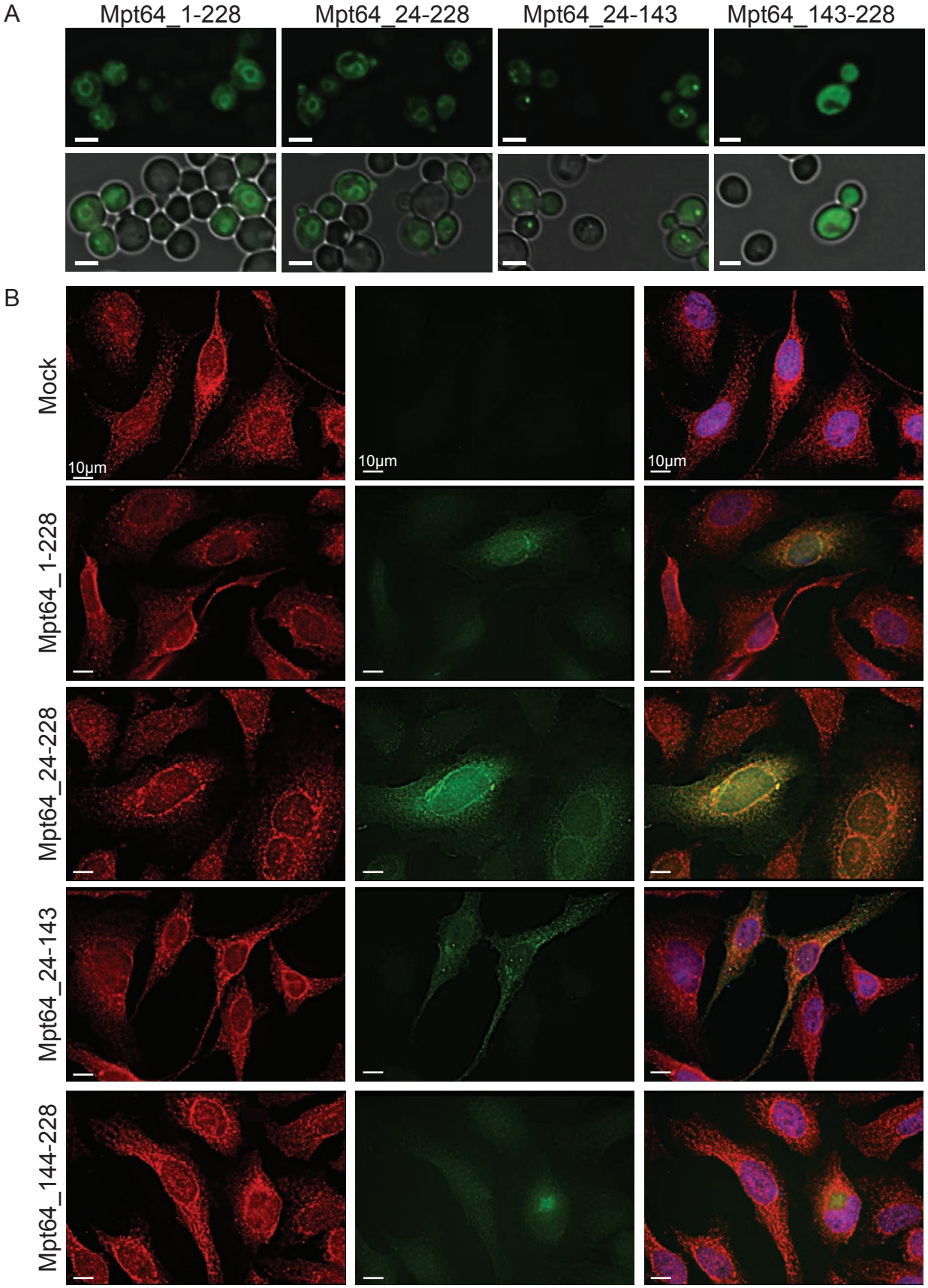

Figure 5. Mpt64 localizes to the endoplasmic reticulum during heterologous expression in yeast and HeLa cells. (A) Immunofluorescence (top panels) and bright field overlay (bottom panels) images of S. cerevisiae transformed with GFP fusion proteins to Mpt64 truncations. Scale bars are 3 µm. (B) HeLa cells transfected overnight with GFP fusion proteins (green) and stained for ER localization with anti-calreticulin antibody (red). Nuclei are stained with DAPI (blue). Scale bars are 10 µm.

Figure 6

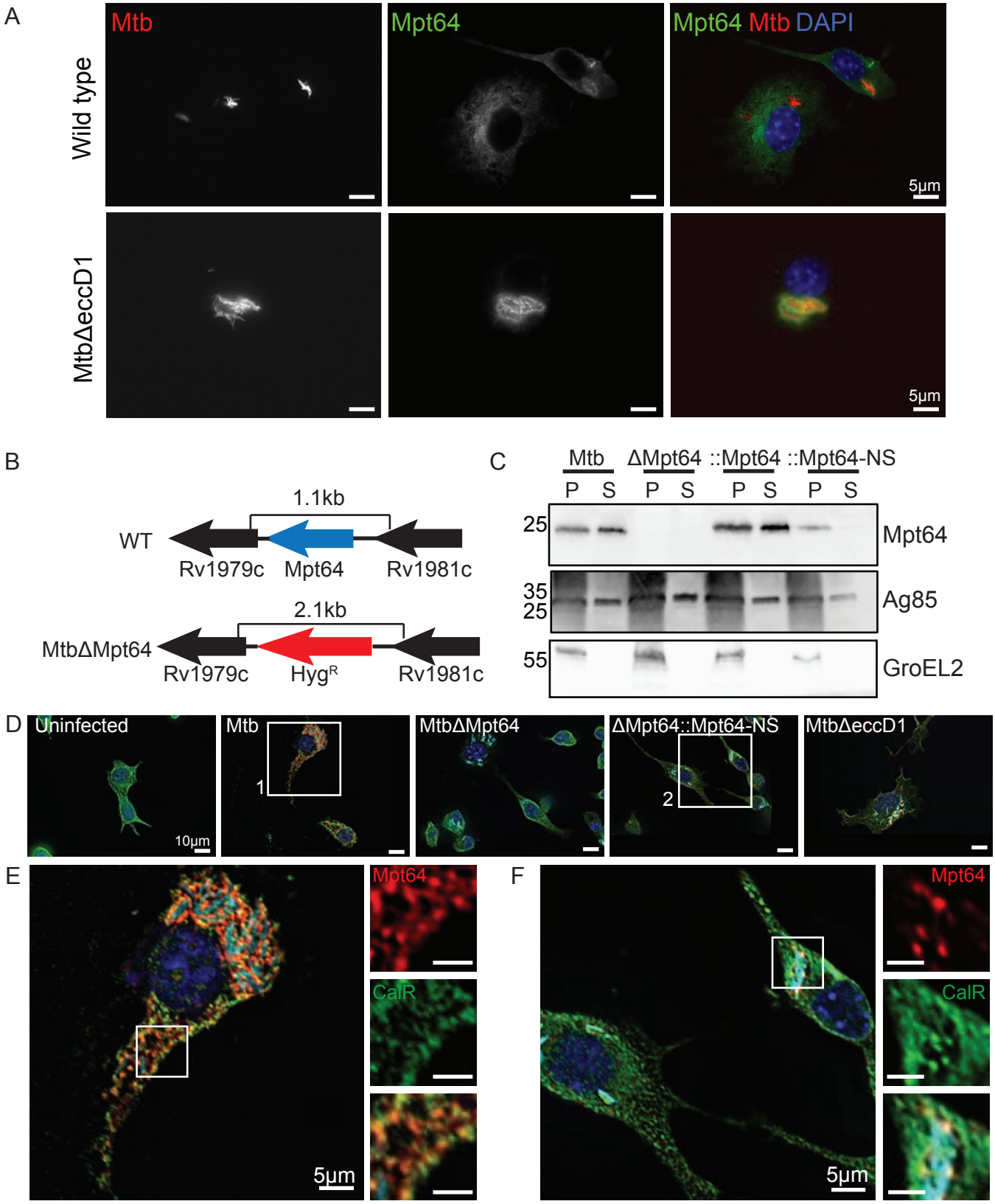

Figure 6. Mpt64 ER localization is ESX1-dependant during M. tuberculosis infection of macrophages. (A) RAW267.4 murine macrophages were infected with mCherry-expressing (red) WT (upper panels) or MtbΔeccD1 (lower panels) for 4 hours at an MOI 20:1. Cells were fixed and stained for Mpt64 (green) and nuclei (blue). Scale bars are 5μm. (B) Schematic detailing in-frame deletion of mpt64 by insertion of a hygromycin resistance gene. (C) Western blot detecting expression of Mpt64, Ag85 and GroEL2 in either the lysate of the cell pellet (P) or culture supernatant (S) of four Mtb strains. (D) RAW267.4 macrophages were infected with the indicated strains of mCherry-expressing (cyan) Mtb for 4 hours at an MOI 20:1. Cells were fixed and stained for Mpt64 (red), calreticulin (green) and nuclei (blue). Images in (E) and (F) correspond to box 1 and box 2, respectively. Scale bars are 10μm. (E) Enlarged image from box 1 in (D) of an Mtb-infected macrophage stained for Mpt64, calreticulin and DAPI. Insets show an area of Mpt64-calreticulin co-localization. Scale bars are 5μm. (F) Enlarged image from box 2 in (D) of macrophages infected with MtbΔMpt64::Mpt64-NS and stained for Mpt64, calreticulin and DAPI. Scale bars are 5 μm.

Figure 7

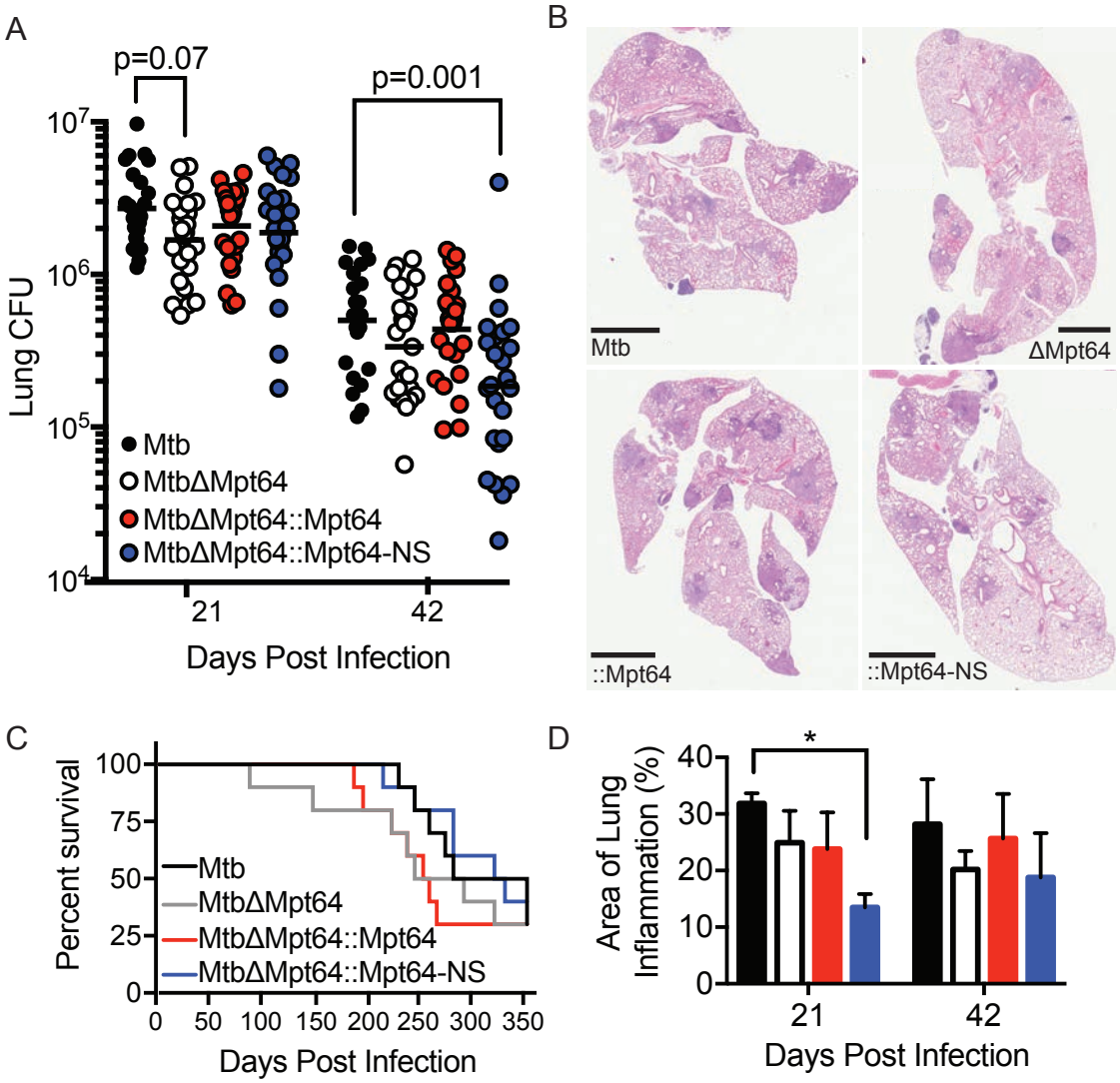

Figure 7. Mpt64 contributes to early Mtb growth after aerosol infection of mice (A) Bacterial burden in lungs of mice 21 and 42 days after aerosol infection with indicated strains of Mtb. Results are a combination of three independent experiments, n=25 mice total per group. Horizontal bar indicates the geometric mean. p values are determined by nonparametric Kruskal-Wallis analysis.
(B) Representative images of H&E stained lungs at 42 days post-infection with the indicated strains of Mtb. Scale bars, 2mm. (C) Ten mice per group were monitored for survival. There were no significant differences in survival rates between groups by Kaplan–Meier analysis. (D) Quantitation of lung inflammation of mice infected with indicated Mtb strains. Measurement was determined using ImageJ software (NIH). Bars are colored as in (A). Results are the mean ±SEM for three animals per group. *p<0.02 by Kruskal-Wallis test.

Figure 8

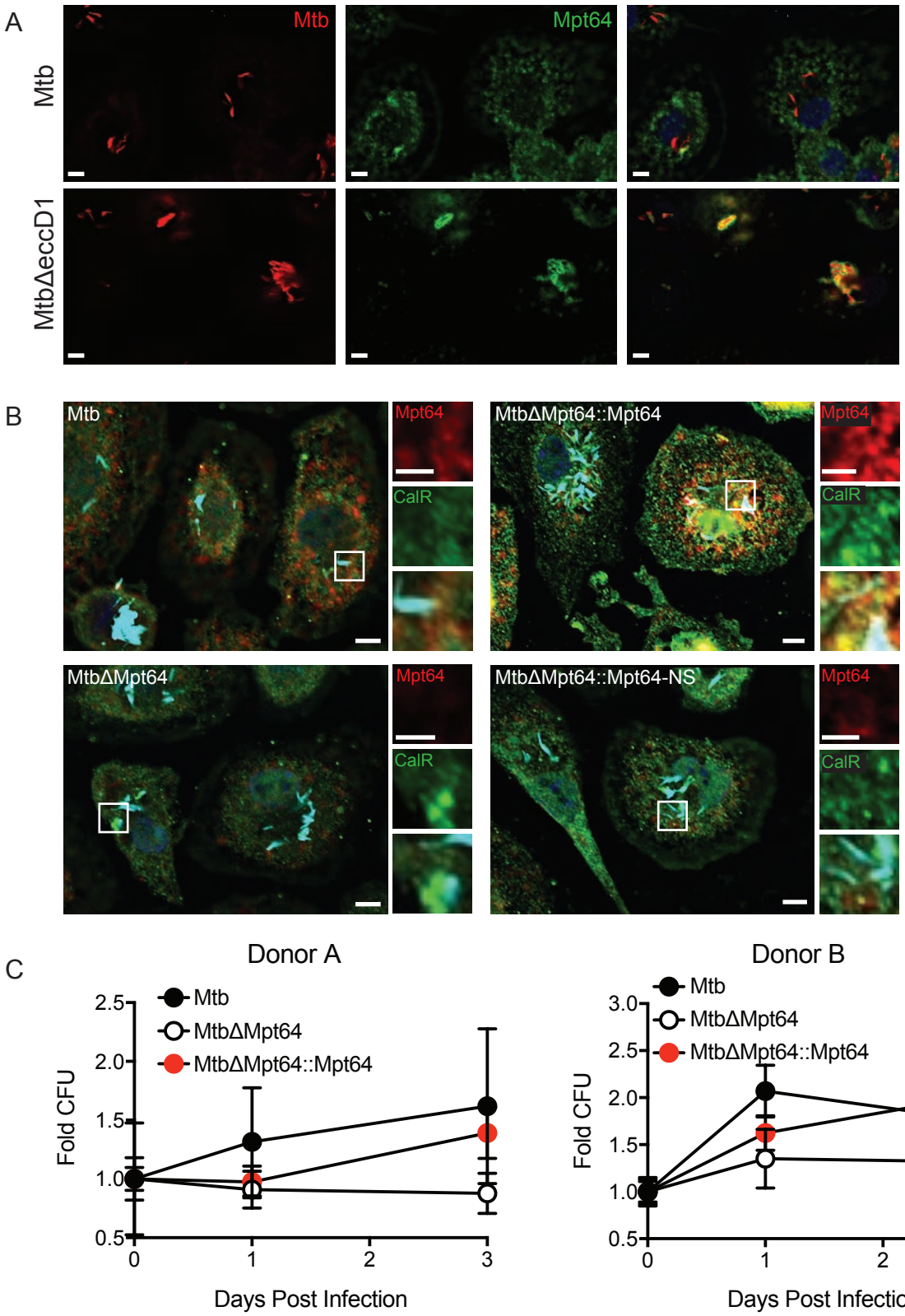

Figure 8. Localization and activity of Mpt64 in human macrophages (A) Primary human monocyte-derived macrophages were infected with mCherry-expressing (red) Mtb or MtbΔeccD1 for 4 hours at an MOI 10:1. Cells were fixed and stained for Mpt64 (green). Scale bars are 5μm. (B) Primary human monocyte-derived macrophages were infected with the indicated strains of mCherry-expressing Mtb for 4 hours at an MOI 10:1. Cells were fixed and stained for Mpt64 (red) and calreticulin (green). Nuclei are stained blue. Scale bars are 5 μm and scale bars of inset images are 2.5 μm. (C) CFU recovered from primary human macrophages from two separate donors infected with Mtb, MtbΔMpt64, or MtbΔMpt64::Mpt64 at indicated time points. CFU was normalized to the bacterial burden at day 0 and is represented as the mean with standard error. Data are representative of 6 independent experiments.